

Investigation of Well Clogging during Managed Aquifer Recharge of Tile Drainage Water

An ASTR Pilot Study

J.F. Ros

In partial fulfillment of the requirements for the degree of

Master of Science
Civil Engineering
Track of Urban Water Engineering

At the Delft University of Technology
To be defended publicly on Tuesday March 30th, 14:00

Supervisor: Ir. E. Kruisdijk, TU Delft
Thesis Committee: Assoc. Prof. Dr. B. van Breukelen, TU Delft
Assist. Prof. Dr. M. Brehme, TU Delft
Prof. Emer. Dr. P.J. Stuyfzand, Stuyfzand Hydroconsult⁺, TU Delft, KWR

An electronic version of this thesis is available at <http://repository.tudelft.nl/>

Table of Contents

Abstract	1
1. Introduction	1
2. Material and Methods.....	4
2.1. Description ASTR Site and Wells	4
2.2. Characterization of the Target Aquifer.....	5
2.3. Description ASTR System and Data Collection	5
2.4. Set-up of the ASTR Infiltration Pilot and Well Rehabilitation	6
2.5. Sampling Procedure.....	7
2.6. Analytical Methods on (Ground)water Samples	8
2.6.1. Water Quality of Injectant (TDW)	8
2.6.2. Well Rehabilitation Sample Processing.....	8
2.6.3. Sample Fluid Fraction.....	8
2.6.4. Sample Solid Fraction.....	9
2.6.5. Mineral Speciation (Identification and Quantification).....	10
2.6.6. Digital Microscope Analysis	10
2.7. ASTR Clogging Investigation and Diagnosis	10
3. Results and Discussion.....	11
3.1. Extent of the Clogging Problem	12
3.1.1. Infiltration Period One (October 31 st to December 11 th , 2019)	12
3.1.2. Infiltration Period Two (September 20 th to October 14 th in 2020)	14
3.1.3. Similarities and Differences between Infiltration Periods and Events	16
3.2. Results on the Injectant Water Quality and Suspended Material (Well Input)	17
3.2.1. Hydrochemical Properties of Recharge Water	17
3.2.2. Biological and Physical Characteristics of Recharge Water	19
3.3. Injection Well Clogging	21
3.3.1. Results of Hydrogeochemical Analysis of Suspended Material (Well Output)	22
3.3.2. Hydrochemical Environment in the Well	23
3.3.3. Results on Particle Size and Microscopic Analysis of Suspended Material.....	25
3.3.4. Clogging Material Composition	26
3.4. Well Rehabilitation Evaluation	26
3.4.1. Camera Inspection	26
3.4.2. Operational Improvement and Considerations	27
3.4.3. Residual Clogging Material.....	27
3.4.4. Alternative Regeneration Methods	27
3.5. Clogging Mitigation Strategies for Breezand and Similar ASTR systems	28
3.5.1. Tile Drainage Network	29
3.5.2. Alternative Pre-treatment.....	29
4. Conclusion and Recommendations	30
Cited References	32

Acknowledgements

I dedicate the work on this manuscript to my Dear mother and father, Elleke and Arjan, and my sisters Suzanne Jeanine, and Laura. Their unconditional support and love remains ever dear to me. My housemates: Goitze, Vesna, Wesley, Tom, and Mira (ex: Chiara and Ian) enduring my thesis rollercoaster - yet often enthusiastic, were simply magnificent in their support. I'm lucky to have them around me. Likewise, I would like to acknowledge my close friends Ioanna, Pablo, Voytek, Sandra, and Sean for their listening ears. My academic writing reviews by Sandra ('Satan') and Voytek are greatly appreciated while Pablo's incredible positive spirit kept my attitude at the upmost. I would, therefore, also like to dedicate my work to the hardships Pablo endured during the Corona pandemic.

The numerous trips to the ASTR pilot in Breezand with night-stays in 'luxury' hotels with Emiel were some of the highlights. Emiel's approachable nature has developed me greatly in the field of academic writing and given me insights and inspiration through his dedicated expertise as a researcher. His hard work and perseverance with the many complicated facets of running and managing a pilot throughout his PhD work deserves the upmost recognition.

Being exposed to the (hydro)geochemical MAR research field Pieter Stuyfzand contributed to significantly, provided a true source of inspiration. As an open book of knowledge during the several meetings, his attentive remarks pushed me in the right directions of my research objectives. It was a pleasure and honour to have him in my committee. Boris and Maren were likewise terrific in their feedback and a pleasure to work with. A special thanks to Maren for her great moral and remarks.

My thesis journey has aspired me to the field of research. As a scholar, I've learnt and been inspired by the best and I'm looking forward to my future career endeavours.

'Count your blessings'

Abstract

This study addresses the critical aspects of injection well clogging as part of an Aquifer Storage, Transfer and Recovery (ASTR) pilot infiltrating tile drainage water (TDW) from agricultural field into an anoxic brackish sandy aquifer for later re-use as irrigation water for flower bulbs. Two ASTR injection periods suffering from clogging were intensely monitored during several weeks in 2019 to 2020. The wells were rehabilitated by methods of backflushing and mechanical cleaning (high-pressure jetting) and sampled to obtain information on the kind of clogging material. The recharge water is nutrient rich (PO_4 : 2-18 mgL^{-1} , NO_3 : 6-50 mgL^{-1} , NH_4 : 0.1-0.55 mgL^{-1} , DOC: 24.5-32.3 mgL^{-1}) and attained significantly turbid conditions (usually between 5-20 NTU; up to 160 NTU) caused by the removal of resuspended biochemical material in the tile drainage network by extreme precipitation and extensive drain discharge events. Consequentially, the 40 μm spin Klin-disc filters as pre-treatment step experienced reduced functionality due to clogging when subjected to high turbid loads. Microbial processes within the ASTR piping system additionally caused fluctuations in turbidity by periodic on/off operation, indicating a high potential for (bio)physical and biological clogging in the injection wells. Microscopic and (hydro)geochemical analysis of injectant and backflushed suspended solids demonstrated a significant contribution of injected Fe-hydroxyapatite flocs and biochemical material incorporating silicious clay and silt particles below 40 μm , while pyrite and possibly calcite precipitants were flushed from the aquifer matrix when removing suspended matter from the wells. The injection of suspended material caused clogging predominantly by physical mechanisms. During standstill, the hydrochemical environment in the well indicated substantial microbial activity by reduced redox conditions in the well and the mobilization of Fe(II), Mn(II), P, and Ca, indicating the vulnerability for biological clogging. Improving the feasibility of the ASTR system requires the high clogging potential of TDW to be reduced. It is recommended to adopt a settling tank, rapid sand filtration followed by slow sand filtration as pre-treatment steps to reduce the physical and biological clogging potential. Various other recommendations to reduce the clogging risks are discussed further. Regarding the well rehabilitation, methods of compressed-air 'jutteren' are recommended to recovery the well performance by effectively removing residual clogging material from the gravelpack and borehole wall.

1. Introduction

Managed Aquifer Recharge (MAR) is becoming a vital water management technique due to increasing water scarcity and global climate change (Stikker, 1998). Water reclamation and appropriate reuse has, therefore, become a critical issue world-wide (Pfeiffer et al., 2000; Bouwer, 2002). The technique provides water storage without loss of valuable land surface area and prevents water loss through evaporation (Page et al., 2018). Aquifer Storage, Transfer and Recovery (ASTR) is one of the methods allowing for excess water to be stored in an aquifer. The method is performed using separate injection and abstraction wells utilizing the aquifer to improve the water quality via physical and biogeochemical processes during infiltration and subsurface transport (Dillon, 2005; Page et al., 2018; Eom et al., 2020). Aquifer Storage and Recovery (ASR), as opposed to ASTR, utilizes a single well for injection and abstraction. In times of water shortage, the water is abstracted for reuse purposes.

A major drawback of MAR, however, relies on the potential for well clogging. Especially in the case for injection wells when source water is of poor quality (Page et al., 2018). Clogging results in a reduction of recharge rates forming a primary operational challenge to the feasibility of MAR systems (Maliva, 2020). Well deficiency takes place within minutes to weeks of operation (Pfeiffer et al., 2000; Olsthoorn, 1982), therefore the wells necessitate rehabilitation to recover recharge rates and thus the well performance (Martin, 2013; Yeong et al., 2018).

The clogging of injection wells can be induced by physical, biological, chemical, and mechanical mechanisms (Martin, 2013). A strong scientific foundation of the clogging phenomena was formed by Olsthoorn (1982) and Pyne (1995), concluding the main forms of clogging problems relate to physical and biological mechanisms. To minimize clogging in injection wells, it is recommended to treat recharge water to a level of drinking water quality (Bouwer, 2002). More specifically, to minimize clogging by physical processes resulting from an accumulation of inorganic (clay, silts, Fe-oxides) and organic solids (microbes and amorphous debris), turbidity levels should be reduced to 1 NTU (Pyne, 1995) or a maximum of 5 NTU (Martin, 2013). Experimental results have concluded recharge water should contain suspended solids below 2 mgL^{-1} to sustain recharge rates (Okubo and Matsumoto, 1983), while concentrations as low as 0.1 mgL^{-1} are recommended in practice (Zuurbier and van Dooren, 2019). The membrane filter index (MFI) is a conventionally physical clogging parameter recommending the MFI of recharge water to be below 3 sL^{-2} to reduce the clogging potential (Schippers and Verdouw, 1980).

Clogging by biological mechanisms can occur due to high concentrations of biodegradable organic material (BDOC) in recharge water (Stuyfzand and Osma, 2019). The process of microbial growth and accumulation of biomass in the well take place close to nutrient-rich water supply such as filter slots and the gravelpack (Olsthoorn, 1982). Treating the water quality for total organic carbon (TOC) below 10 mgL^{-1} (Olsthoorn, 1982), dissolved organic carbon (DOC) below 2 mgL^{-1} (Zuurbier and van Dooren, 2019), assimilable organic carbon (AOC) below $10 \mu\text{g acetate-CL}^{-1}$ (van der Kooij, 1992), ammonium below 0.5 mgL^{-1} (Hubbs, 2006), and fully eliminating high concentrations of nitrate and phosphate minimize the clogging potential by biological mechanisms (Stuyfzand and Osma, 2019; Eom et al., 2020).

Chemical clogging can occur due to the precipitation of calcium carbonates, Fe-oxides, phosphates, and other minerals (Martin, 2013). Mineral precipitation are often mediated by microorganisms, therefore, making it difficult to distinguish chemical from biological mechanisms (Pfeiffer et al., 2000; Martin, 2013). If the recharge water is saturated with calcite, a coating layer of calcium carbonate can form on aquifer fines in the vicinity of the well (Olsthoorn, 1982). Other mineral precipitants like Fe-oxides occur mainly at the mixing zone of oxic recharge and native groundwater further from the well, suggesting chemical clogging to be less detrimental than physical or biological mechanisms. Total iron concentrations of recharge water are recommended to be below $10 \mu\text{gL}^{-1}$ to minimize chemical clogging by iron precipitants (Zuurbier and van Dooren, 2019). Clogging by clay swelling or dispersion is another facet of chemical and physical mechanisms and can cause rapid clogging. Mobilisation of interstitial fines from clay swelling may be more prevalent when fresh water (low sodium adsorption ratio (SAR)) is recharged into a brackish or saline (high SAR) groundwater system (Olsthoorn, 1982; Martin, 2013). It is a concern when clay content in the aquifer (at least 1%) contain swelling clays like montmorillonite (Olsthoorn, 1982). While lab core testing by Torkzaban et al. (2015) showed a reduction in permeability was negligible with low clay contents (2 to 3%). A SAR of infiltration water below 6 is advised (Zuurbier and van Dooren, 2019). Mechanical clogging is caused by infiltrating entrained air or by the production of biogenic gasses (e.g. nitrogen or methane) within the aquifer by microbial activity (Martin, 2013). The mechanisms cannot be distinguished as separate processes because clogging is induced by an interrelation of these mechanisms, making it necessary to evaluate the contributing as a whole (Pfeiffer et al., 2000; Martin, 2013).

Nevertheless, the noncompliance of treated recharge water to clogging mitigation guidelines does not imply clogging development has to occur. For example, a study has shown suspended solids exceeding 25 mgL^{-1} have not caused clogging in a calcareous aquifer at a stormwater ASR site in South Australia (Pavelic et al., 1998). Physical clogging and the rate of clogging is strongly affected by the particle size of both the aquifer sediment and suspended solids in recharge water (Wang et al., 2016) and emphasises the fact that site-specific factors predominantly govern the clogging potential. These factors consist of: (1) the water quality of injectant, (2) the injection rate (Stuyfzand and Osma, 2019),

(3) the extent of pre-treatment applied, (4) target aquifer characteristics and interaction with reactive geochemical properties (Olsthoorn, 1982), (5) the site-specific geohydrology (Medina et al., 2013), and (6), improper well commissioning and maintenance (Martin, 2013). A direct comparison between clogging field studies is, therefore, of little significance and thus requires site-specific research and investigation.

A recently demonstrated ASR clogging study by Stuyfzand and Osma (2019) on injecting recycled water to a brackish, anoxic sand aquifer in Melbourne, Australia used microscopic and geochemical analysis on suspended solids in the injectant and backflushed water to diagnose the main clogging causes. An analysis was conducted on the contribution of injectant and aquifer particles concluding a significant contribution of diatoms, algae and colloidal or precipitating $\text{Fe}(\text{OH})_3$, $\text{Al}(\text{OH})_3$ and MnO_2 . Moreover, the hydraulic data from the intensively monitored ASR scheme was used to support the clogging problem. Considering the use of recycled water (non-potable) and the 20 μm spin Klin-disc filters and 1-5 μm bag filter in series, mitigation and prevention strategies were proposed.

This study addresses the critical aspect of well clogging in a new ASTR pilot in the Netherlands. Acacia Water Institute and TU Delft are conducting research on a new concept (AGRIMAR) utilizing tile drainage water (TDW) as source water. When excess water is available from precipitation events, the water is injected to a confined, brackish anoxic fine-grained to middle-coarse sandy aquifer in coastal agricultural polders treated for pathogens. When water demands are high, the water can be abstracted and reused for irrigation purposes. Source water is supplied by a subsurface tile drainage network that regulates groundwater to prevent crop deterioration by water damage. Conventionally, the drains discharge to surrounding surface waters (canals), however, tightening environmental regulation and increasing freshwater scarcity encourage the implementation of new water management techniques. A previous ASTR pilot at the same trial site has confirmed the viability. As opposed to the previous ASTR pilot, the new pilot utilizes 40 μm spin Klin-disc filters instead of sand filtration. The alternative treatment was implemented for testing purposes by upscaling the field site (from 2 ha. to 10 ha.). After the first infiltration period between October 31st to December 11th, 2019 (5.5 weeks) injecting 1370 m^3 per well, it was apparent the injection wells suffered from a rapid clogging development. The injection wells were rehabilitated by backflushing and mechanical cleaning (high-pressure jetting) to recover the well performance, but the ASTR system again suffered from rapid clogging in the following infiltration period between September 21st to October 14th, 2020 (3.5 weeks) injecting 1430 m^3 per well. This occurred regardless of an installed automated back-flushing system in the injection wells to prevent clogging.

Numerous studies have investigated the clogging of injection wells by injecting suitable water sources (Pfeiffer et al., 2000; Page et al., 2011; Camprovin et al., 2017; Stuyfzand and Osma, 2019). To the best of the author's knowledge, no clogging studies have been performed on injecting nutrient rich TDW (PO_4 : 2-18 mgL^{-1} , NO_3 : 6-50 mgL^{-1} , NH_4 : 0.1-0.55 mgL^{-1} , DOC: 24.5-32.3 mgL^{-1}) and the potential for clogging. Considering the benefit for farmers to adopt the water management technique, an understanding of the clogging potential utilizing TDW is warranted. Accordingly, this study performs a clogging investigation using similar methods to Stuyfzand and Osma (2019). The objectives of this study are to: (1) Evaluate the clogging potential of TDW to clogging mitigation guidelines and the impact the current 40 μm Klin-disc filters provide to reduce the clogging risks. (2) Diagnose the main clogging mechanisms occurring in the ASTR system and the factors that enhance clogging development. (3) Evaluate the well rehabilitation by the applied regeneration methods to assess their suitability. And (4), provide learnings from the study and recommend improvements to the current ASTR pilot and similar systems to reduce the clogging potential. To this end, hydraulic, hydrogeochemical, geochemical, and microscopic data were obtained and analysed.

2. Material and Methods

2.1. Description ASTR Site and Wells

The trial site lies in a coastal agricultural polder in the town of Breezand located in the Province of North-Holland (Fig. 2.1a). The ASTR system is supplied by tile drainage water (TDW) discharged from a 10 ha. flower bulb field when excess water is available (Fig. 2.1b). The tile drainage network is situated 80 cm below ground level (BGL) and discharges TDW to a drain reservoir regulating the water level in the irrigation field. The topsoil consists of mainly fine sand from surface level (-0.1 m NAP) to approximately 2.2 m BGL (TNO lithological site survey, 2018 in the supplementary data (SD) adopted from E. Kruisdijk, Section 1).

The ASTR system started operation in October 2019 and consists of two injection and four abstraction wells (Fig. 2.1c). The injection well, screened between 11.5-33 m BGL (long filter) and abstraction well, screened between 12-23 m BGL, are each equipped with a piezometer inside the gravelpack, approximately 35 mm and 50 mm distance to the well screen, respectively. The piezometer is screened at 20.5-22.5 m BGL with 0.5 mm slot size and of PVC material. The injection well, of PVC material, has an inner diameter of 110 mm for the well riser to a depth of 11.5 m, and 100 mm for the well screen to 33 m BGL with 0.5 mm filter slot size. The annular gravelpack width is 70 mm and consists of 800-1200 μm packing material surrounding the well screen. The total bore diameter is 240 mm, with an infiltration surface area of 17 m² to the aquifer. A nested monitoring well is used for sampling at six depths between 12 m and 32 m BGL in the target aquifer.

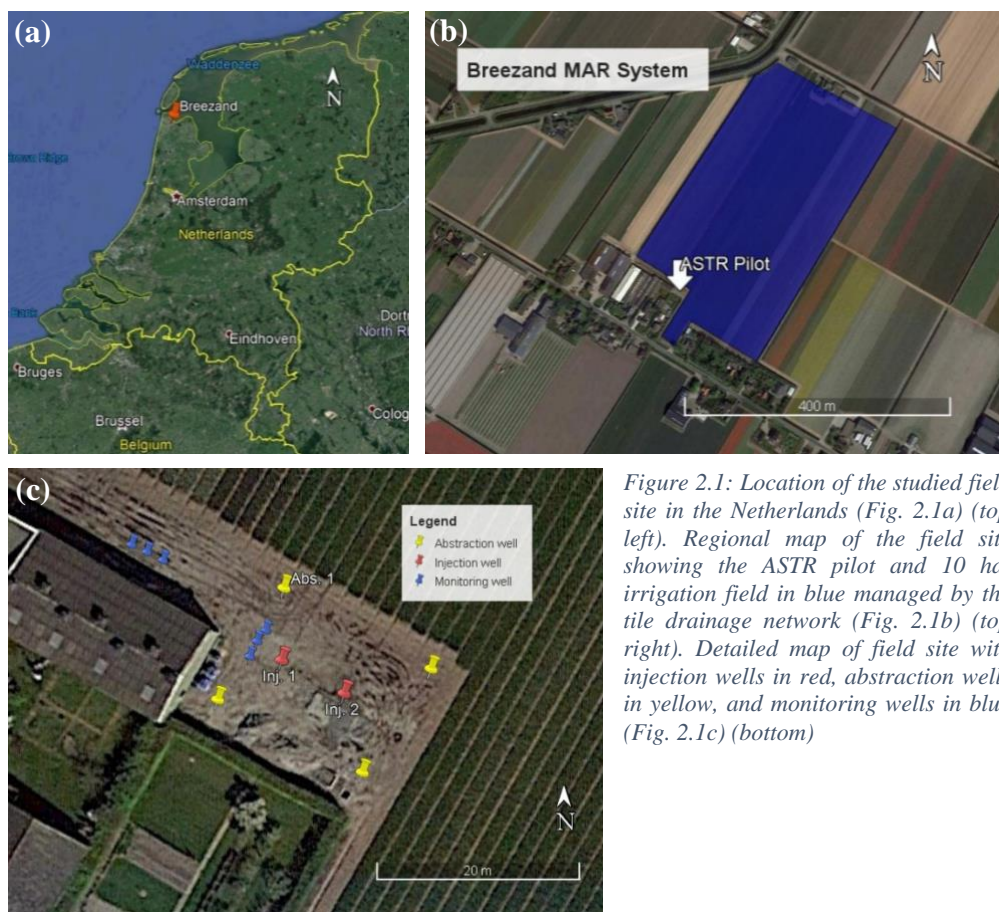


Figure 2.1: Location of the studied field site in the Netherlands (Fig. 2.1a) (top left). Regional map of the field site showing the ASTR pilot and 10 ha. irrigation field in blue managed by the tile drainage network (Fig. 2.1b) (top right). Detailed map of field site with injection wells in red, abstraction wells in yellow, and monitoring wells in blue (Fig. 2.1c) (bottom)

2.2. Characterization of the Target Aquifer

The ASTR target aquifer is confined and sequenced by three strata of unconsolidated sand deposits (formation of Boxtel, Eem and Drenthe) of late Quaternary age. Average sedimentological and geochemical analysis on the aquifer matrix show predominantly fine sand (125-250 μm) for the upper well screen and predominantly medium coarse (250-500 μm) for the remaining well screen depth (SD. Fig. 1.1). Sedimentary organic material is present throughout the aquifer averaged at 1% dry weight (% d.w.) with averaged pyrite and carbonate traces at respectively, 0.1% d.w. and 3% d.w. The Upper Eem formation (shallow marine deposit) at approximately 16 m BGL contains the highest content of pyrite and carbonate at respectively, 0.4% d.w. and 11% d.w. The average clay content within the aquifer is deduced from %lutum ($< 2 \mu\text{m}$) quantified through aquifer core analysis by TNO. Throughout the aquifer no sediments were classified below 2 μm , indicating clay content is negligible and thus at $\sim 0\%$ d.w. No blind casing was used along the filter screen due to the predominant homogeneous sand content.

The native groundwater, before initiation of the first infiltration period, was deeply anoxic (NO_3 and SO_4 depleted) and showed a clear salinity stratification across the hydrochemical depth profile (1860 to 8930 $\mu\text{S}/\text{cm}$) between 12 m and 32 m BGL, respectively. Chemical constituents over depth respectively show; Cl^- (440-2760 mgL^{-1}), Fe^{2+} (9.5-39 mgL^{-1}), Na^+ (200-650 mgL^{-1}), Mg^{2+} (30-205 mgL^{-1}), K^+ (9-57 mgL^{-1}) and Ca^{2+} (200-1515 mgL^{-1}). The Sodium Adsorption Ratio (SAR) of native groundwater ranges between 1.0 and 0.8 across the sampled depth. The potentiometric water level in the confined aquifer is at an elevation of approximately 50 cm BGL and has an average ambient water temperature of 11.5 $^\circ\text{C}$.

2.3. Description ASTR System and Data Collection

A schematic of the ASTR system is presented in Figure 2.2. The tile drainage network regulates the groundwater level in the field when water is supplemented by precipitation events. The excess water is discharged and fills the drain reservoir at the main tile outlet (Fig. 2.2). Depending on the duration of drainage events, related to the intensity of precipitation events, the availability of TDW can vary significantly. Level indicators (LI. 1 and 2, Fig. 2.2) within the drain reservoir regulate the field drainage by respectively discharging water to the ASTR system and/or discharging to the surrounding surface

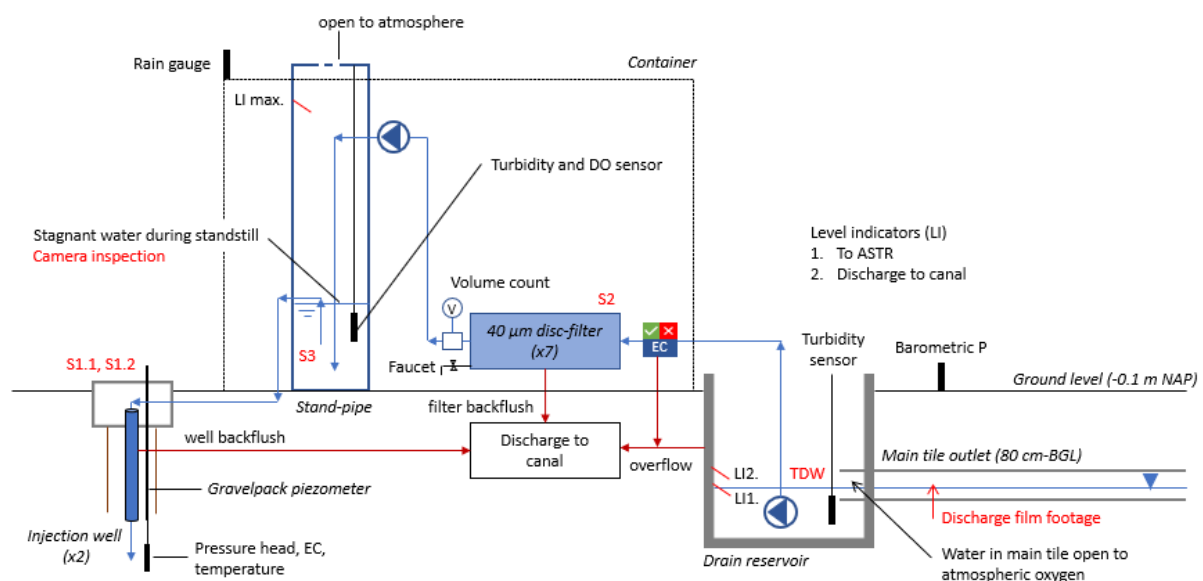


Figure 2.2: A schematic representation of the ASTR system (injection well) in Breezand from main tile outlet, pre-treatment, and injection well. Annotations provide information on system operation and data monitoring. TDW, S1.1, S1.2, S2, and S3 represent sample locations within the system described in Section 2.5.

water (canal). Because the injectant capacity is limited to 24 m³/h (12 m³/h per well), exceeding drainage rates can cause simultaneous discharge to the ASTR system and to the surrounding surface water.

Water from the drain reservoir to the ASTR system is regulated by an electric conductivity (EC) threshold. If exceeded, the recharge water is discharged to the surrounding surface water (Fig. 2.2). Permissible recharge water is routed via the 40 µm spin Klin disc-filter manifold and fills the standpipe. When a pressure differential (ΔP) is reached over the disc-filter manifold due to clogging, an automatic backflush is initiated, discharging the wastewater to the canal (Fig. 2.2). Moreover, in case of a calamity, a faucet below the disc-filters allow stagnant water to be removed. The pre-treated recharge water fills the standpipe to approximately 2 m standing head for infiltration under gravity. The standing head is maintained by a level indicator in the standpipe that supplies recharge water from the drain reservoir to standpipe in an order of seconds. Probes within the standpipe measure the following parameters in 10-minute intervals: turbidity (NTU) and dissolved oxygen (DO mgL⁻¹) (Ponsel NTU sensor; Ponsel OPTOD sensor, Bell Flow Systems, Buckingham, Great Britain). The sensors are always submerged due to a constant minimum water level in the standpipe (Fig. 2.2). The volume injected (m³) is measured by the volume count prior to infiltration (Fig. 2.2) and expressed in total volume for infiltration period one. The accumulated volume injected in infiltration period two was noted periodically in discrete intervals. The recharge flow (m³/h) was not measured in period one and was monitored periodically as discrete intervals in period two. The recharge flow for both periods was derived from a linear regression (flow correlated to head rise at distance [n = 46, R² = 0.9], SD, Fig. 2.6). On December 10th, 2020, a turbidity sensor was installed within the drain reservoir (Fig. 2.2). A rain gauge (tipping bucket, 0.2 mm intervals) on top of the container monitors precipitation at a frequency of 10-minutes.

Within the gravelpack piezometer, a datalogger (CTD diver, Van Essen, Delft, Netherlands) collects data on pressure head (cm H₂O), EC (µS/cm) and temperature (°C) for injection well one, two and abstraction well one. Moreover, a datalogger in a piezometer on the field-site monitors the phreatic water level (cm H₂O). The barometric pressure (cm H₂O) measured at ground level is used to correct the down-hole pressure. This provided the hydraulic data for the wells and phreatic water level (cm H₂O) at a frequency of 15-minutes. Due to the limited temperature difference between injectant (average injectant temperature: 12 °C) and ambient groundwater (11.5 °C), no temperature correction for viscosity was applied.

2.4. Set-up of the ASTR Infiltration Pilot and Well Rehabilitation

Clogging of injection well one and two was investigated using the gravelpack piezometer relative to a dedicated monitoring well in the gravelpack of abstraction well one (Fig. 2.1c). The respective distance for injection well one and two to the monitoring well was 7 m and 11 m, respectively. This set-up was chosen because of the symmetrical configuration of the ASTR wells and because clogging did not occur at the abstraction well during infiltration. The first operation of the ASTR pilot was conducted between October 31st to December 11th, 2019 with clean wells meaning injection initially performed at design capacity of 12 m³/h per well. In total 1370 m³ was infiltrated per well over 20 days of infiltration runs. At the end of the period the injection wells were severely clogged and underwent rehabilitation on February 2nd to 4th, 2020 after the system stood still for 82 days.

The well rehabilitation was performed by the following regeneration cycle: (1) an initial backflush at 11 m³/h, (2) mechanical cleaning by high-pressure jetting nozzles (100-200 bar, Fig. 2.3) and simultaneous discharge at 3 m³/h. The

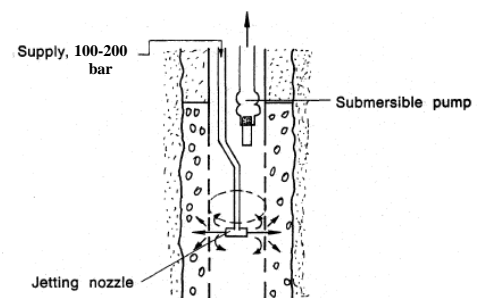


Figure 2.3: Schematic of high-pressure jetting procedure. Adopted and modified from Olsthoorn (1982)

well screen was cleaned from top to bottom and back (0.20 cm/min, 1-hour procedure). (3) a post backflush at 11 m³/h. After the initial backflush, a buffer was filled with approximately 3 m³ abstracted water for the mechanical cleaning procedure.

In July 2020 a backflush system was installed with a fixed pump at 9 m depth in injection well one and two. The backflush regime would provide a 15-minute backflush (20 m³/h) after consecutive injected volumes of 150 m³ per well. In filtration period two in September 2020, after two weeks of operation, the backflush regime was intensified to performing a backflush after injecting 50 m³. This was done because the injection wells experienced rapid clogging.

The second infiltration period between September 21st to October 14th, 2020 infiltrated 1430 m³ per well over 20 days of infiltration runs. At the end of the period, the wells were again rehabilitated by mechanical methods (high-pressure jetting at 120 bar) from bottom to top filter screen (5-minute procedure) on November 25th, 2020 after the system stood still for 45 days. A submerged pump in the well riser discharged the material with 8 m³/h after the mechanical cleaning procedure.

2.5. Sampling Procedure

TDW, S1.1, S1.2, S2, and S3 codes denoted in Figure 2.2 represent sample locations within the ASTR system. Figure 2.4 summarizes the sampling in a timeline in relation to the two infiltration periods and well rehabilitations performed during the study.

Tile drainage water samples (TDW)

In total 19 TDW samples were taken in 1 L glass bottles from the drain reservoir during discharge events. Six of the samples were taken daily during the first infiltration period in November 2019. Five monthly samples were taken in December 2019, January, February, May, and July 2020. Eight samples were taken weekly in the second infiltration period in October and November 2020. All samples were cooled to 4 °C immediately after sampling.

Well rehabilitation samples (S1.1 and S1.2)

The well rehabilitation on February 2nd to 4th 2020 was intensively sampled following methods of Olsthoorn (1982). Specifically, the first backflush and the mechanical cleaning procedure. Rehabilitation field studies by Olsthoorn (1982) conclude the first several backflush samples provide information on the clogging composition. Because the injection wells in Breezand did not experience backflush events prior to the well rehabilitation, the method deemed suitable to obtain information on clogging by removing suspended material from the well. Sampling was performed by considering the volume pumped at 11 m³/h and well volume specifications regarding riser volume (90 L), standing well volume (riser + well screen: 270 L) and borehole volume (riser + well screen + annular gravelpack: 970 L). This provided an indication on sampling points in time during the backflush. The camera was simultaneously maintained at 9 m depth in the well during pumping and provided visual conditions during sampling. The samples were corrected on the time delay between pumping and discharge at the drain reservoir functioning as dedicated sampling point. During the mechanical cleaning procedure, the submersible camera could not be used but the downward nozzle speed was used to pinpoint approximate sample locations along the well screen. After every regeneration procedure, the camera was used to inspect the in-well conditions from top to bottom. The well rehabilitation sampling on November 26th, 2020 was performed differently. Once the high-pressure nozzles cleaned the filter slots and the well interior, the wastewater was removed and discharged to the drain reservoir. The bulk clogging material was sampled at the drain reservoir.

17 samples were taken in 10 L PE jerry cans during the first well rehabilitation in February 2020 (S1.1) while 3 samples were taken in 10 L glass bottles in November 2020 (S1.2). The samples were coded and directly placed in the farmers cool cell (5 °C) before transfer to the TU Delft cool cell (8 °C).

Disc-filtrate and standpipe material samples (S2 and S3)

Samples S2 and S3 refer to filtrate material removed from the disc-filters and removal of material on the interior of the standpipe, respectively. The submersible camera was used to investigate the conditions within the standpipe, alongside conditions within the main tile outlet during a 3-minute discharge event. S2 and S3 material was removed using a PE spatula, demi-rinsed into PE containers and subsequently stored in an on-site refrigerator at 4 °C.

2.6. Analytical Methods on (Ground)water Samples

2.6.1. Water Quality of Injectant (TDW)

On site, pH and EC was measured from the 1 L TDW samples. Samples for further hydrochemical analysis were passed over 0.45 µm cellulose acetate membrane (Whatman Spartan 30/0.45RC syringe) in the field and stored in a 10 mL and 50 mL plastic vial. The 10 mL vial was acidized using 1% HNO₃ solution for analysis of cations and trace elements (As, B, Ba, Ca, Co, Cr, Cu, Fe, K, Li, Mg, Mn, Mo, Na, Ni, P, Pb, S, Sb, Se, Sr, Ti, V and Zn) using Inductively Coupled Plasma – Mass Spectrometry (ICP-MS; PlasmaQuant MS, Analytik-Jean, Germany) at the TU Delft Lab. The 50 mL vial was used for analysis on anions and trace elements (Ac, Br, Cl, F, NO₂, NO₃, PO₄, SO₄) using Ion Chromatography (883 Basic IC Plus; Metrohm AG, Herisau, Switzerland). Alkalinity (as HCO₃) was determined by potentiometric titration (702 SM Titrino, Metrohm AG, Herisau, Switzerland) using HCl as reagent. DOC was determined using the total organic carbon analyser (TOC-V CPH, Shimadzu, Japan) at TU Delft. PHREEQC (Parkhurst and Appelo, 1999) was used to model the saturation states of injectant water using the standard PHREEQC database.

The dissolved oxygen content (mgL⁻¹) and turbidity (NTU) measured in the standpipe was used to determine the physicochemical injectant properties during infiltration runs. The injectant temperature (°C) was obtained from dataloggers (CTD diver) within the injection well.

2.6.2. Well Rehabilitation Sample Processing

The 17 samples (9.5-10.7 L) in the TU Delft cool cell (8°C) were kept idle in the dark for three to six days to allow suspended material to settle. Separating the fluid fraction (supernatant) from the wet clogging residue (slurry) was done through decanting using a peristaltic pump, transferred to a clean demi-washed 10 L PE jerrycan. The remaining slurry in the original jerry can (0.5 - 1 L) was transferred to 1 L borosilicate glass bottles and demi-rinsed to transfer all the material. Using a digital scale (PG2002-S Delta Range, Mettler Toledo, Ohio, United States) all intermediate weights were noted for a mass balance (±0.01 g).

2.6.3. Sample Fluid Fraction

After separating the supernatant, the EC (µS/cm), pH, temperature (°C) and turbidity (NTU) was measured with calibrated probes (EC, pH and temperature: respectively, InoLab Multi 720 and InoLab Multi 9420, WTWTM, Weilheim, Germany. Turbidity: HACH 2100N Turbidimeter, Colorado, United States). All measurements were converted to 20 °C and 25 °C to respectively determine: (1) the sample fluid density by considering temperature and residue of evaporation (RE). This was performed to convert the mass of sample supernatant to volume ($V = m\rho^{-1}$). The method was performed using Stuyfzand's algorithm (1993), suitable for EC <1500 µS/cm (Pers. Comm. Vincent Post) by: ρ (kgL⁻¹)

$= 1 + (8.05 \times 10^{-7}) \times RE - (6.5 \times 10^{-6}) \times (t - 4 + 2.2 \times 10^{-4} \times RE)^2$, where t = temperature ($^{\circ}\text{C}$) and $RE = 0.69778 \times EC_{20}$. (2) determine the total dissolved solids (TDS) from EC_{25} . Using the standard correction factor $K = 0.7$ for fresh water (Walton, 1989), the TDS was derived by $TDS (\text{mgL}^{-1}) = EC_{25} (\mu\text{S}/\text{cm}) \times K$. The TDS was compared to the ionic balance assuming equilibrium within the fluid fraction and showed results deviated by $\pm 10\%$.

At the TU Delft lab, 10 mL and 50 mL aliquots of each samples' supernatant was passed over 0.45 μm . The 10 mL aliquot was diluted 1:20 using 1% HNO_3 ICP-MS stock solution for cation analysis using ICP-MS. The 50 mL aliquot was used for anion analysis using IC. 30 mL aliquots were prepared for dissolved organic carbon (DOC) analysis using the Laboratory of Sanitary Engineering, TU Delft protocol for the total organic carbon analyser (TOC-V CPH, Shimadzu, Japan). This yielded the fluid-elemental content (mgL^{-1}) of each sample.

2.6.4. Sample Solid Fraction

The remaining slurry in the 1 L borosilicate glass bottles was processed by oven heating at 105°C for 72 h to evaporate the remaining fluid-fraction and determine the total solids (TS) by weight. The residue of evaporation is accounted for later in this section. The weight moisture content was considered by cooling the sample to room temperature before applying the mass balance. The dry material (1.0-65.0 g) was transferred to 35 mL PE screw top containers and transported to the lab at the Vrije Universiteit (VU) in Amsterdam. Here, 1 gram of the material was crushed and homogenized. 10 milligrams was used for the C/N analysis by first dissolving carbonates with acid. For the particle size (sediment) analysis, several grams of uncrushed material was prepared in 1 L glass beakers. The organic content was first oxidized with 5 mL H_2O_2 in 100 mL demi water, catalysed by heat until completely oxidized. The samples were subsequently cooled to 40°C and treated with 5 ml 10% HCl for dissolution of iron-oxides and carbonates. Once leached, 900 mL demi water was added to the solution, covered, and settled overnight. The samples were then decanted and a dispersant ($\text{Na}_4\text{P}_2\text{O}_7 \cdot 10\text{H}_2\text{O}$) was added to disaggregate clay particles. Finally, the samples were analysed by laser diffraction (Helos KR wet particle analyser, Sympatec GmbH, Clausthal-Zellerfeld, Germany).

At the TU Delft, 30 ± 0.01 mg (AT261 DualRange, Mettler Toledo, Ohio, United States) of crushed and homogenized material of each sample was digested with nitric acid (APHA method 3030E). A 100 mL flask was placed on a heat plate and material was transferred by rinsing the dish and funnel with ultra-pure water (ELGA Ultra AN MK2, VWR TM, the Netherlands) into a flask. 5 mL 69% HNO_3 (Titripur®, Darmstadt, Germany) was added to a flask and diluted to 20 mL with ultra-pure water and heated to 95°C . Once all leachable material was dissolved, the digestion was complete and diluted to 100 mL with ultra-pure water. A 10 mL aliquot was subsequently diluted 1:50 using 1% HNO_3 ICP-MS stock solution, passed over 0.45 μm , and analysed for cations using ICP-MS. A 50 mL aliquot was prepared, passed over 0.45 μm , and analysed for anions using IC. This yielded the solid-elemental content (mgL^{-1}) of the total solids digested.

The total suspended solids (TSS) for each sample was achieved by correcting the total solids for total dissolved solids by: $TSS (\text{mg}) = TS (\text{mg}) - [TDS (\text{mgL}^{-1}) \times \text{sample volume of supernatant (L)}]$. Quantifying the solid-elemental constituent in %d.w of total suspended solids first required a weight ratio (%) between constituent X (mgL^{-1} by ICP-MS) and digested material (30 ± 0.01 mg) in 100 mL solvent to be determined:

$$\text{weight ratio (\%)} = \frac{\text{Constituent X (mgL}^{-1}) \times 0.1L}{\text{digested material (mg)}}$$

The correction for residue of evaporation during sample heating can now be applied. Denoting the total suspended solids in the 1 L sample as X_{SS} , the total solids as X_{TS} , and the required correction for dissolved constituents as $X_{\text{H}_2\text{O}}$, the following formulae are applied:

$$X_{TS} (mg) = \%weight\ ratio\ constituent\ X \times TS (mg)\ of\ sample$$

$$X_{H_2O} (mg) = dissolved\ constituent\ X (mgL^{-1}) \times evaporated\ volume (L)$$

$$X_{SS} (mg) = X_{TS} (mg) - X_{H_2O} (mg)$$

$$X_{SS} (\%d.w.) = \frac{X_{SS}(mg)}{TSS (mg)} \quad (1)$$

2.6.5. Mineral Speciation (Identification and Quantification)

Methods of Stuyfzand and Osma (2019) and the decision tree of van Beek (2010) was used to assign each chemical constituent to a mineral by converting the %d.w. to mg/kg by %d.w. \times 10,000. This made the quantification more manageable. Identified minerals >1 %d.w. were considered in this study.

An XRD analysis was performed on two samples, one corresponding to the initial backflush and one from the mechanical cleaning procedure. The XRD was conducted by the lab technician at the XRD and XRF lab at the Mechanical Engineering Faculty (3ME), TU Delft. Maren Brehme subsequently processed the raw data file and interpreted the mineral species.

2.6.6. Digital Microscope Analysis

A digital ‘light’ microscope (VHX-5000 series, Keyence, Mechelen, Belgium) at the TU Delft was used on samples S1.1, S1.2, S2 and S3. 20-200x and 100-1000x magnification lenses were used together with the polarization filter to enhance contrast in micrographs. Polarization, for example, may distinguish frustule transparent cell walls comprised of silicon dioxide in algae (diatoms).

2.7. ASTR Clogging Investigation and Diagnosis

Figure 2.4 and Table 2.1 summarize the investigation in a timeline of the study. The clogging potential of tile drainage water as injectant source is evaluated on a suite of physicochemical parameters regarding clogging mitigation guidelines from literature. The impact of the 40 μ m Klin-disc filter in the pilot is evaluated on its viability to reduce the physical clogging potential. Considering the infiltration under gravity maintaining a constant hydraulic head in the standpipe, the risk of ASTR operation failure over the short term was considered by the deterioration of hydraulic performance during the two infiltration periods. The difference in hydraulic head rise method by Pyne (1995) is used to evaluate the clogging development. Moreover, the change in hydraulic head within the injection well gravelpack piezometer to that of the gravelpack piezometer in the abstraction well (dedicated monitoring well) at distance, was used to investigate the primary clogging location. An injectivity index ($m^3/h/bar$) by methods of Brehme et al. (2018) show the extent of the clogging problem in relation to implicating events during the infiltration periods. The index expresses a change in recharge flow to downhole pressure in response to clogging. Extensive submersible camera inspections aid in the recovering effects of the well rehabilitation and support the localization of clogging.

The geochemical and microscopic analysis on backflushed suspended solids following similar methods of Stuyfzand and Osma (2019) to support the clogging diagnosis. The main clogging mechanisms are concluded by (hydro)geochemical and microscopic analysis on injectant and backflushed suspended material. In combination with the typical clogging processes indicated by the head rise trends. (Olsthoorn, 1982; Pyne, 1995).

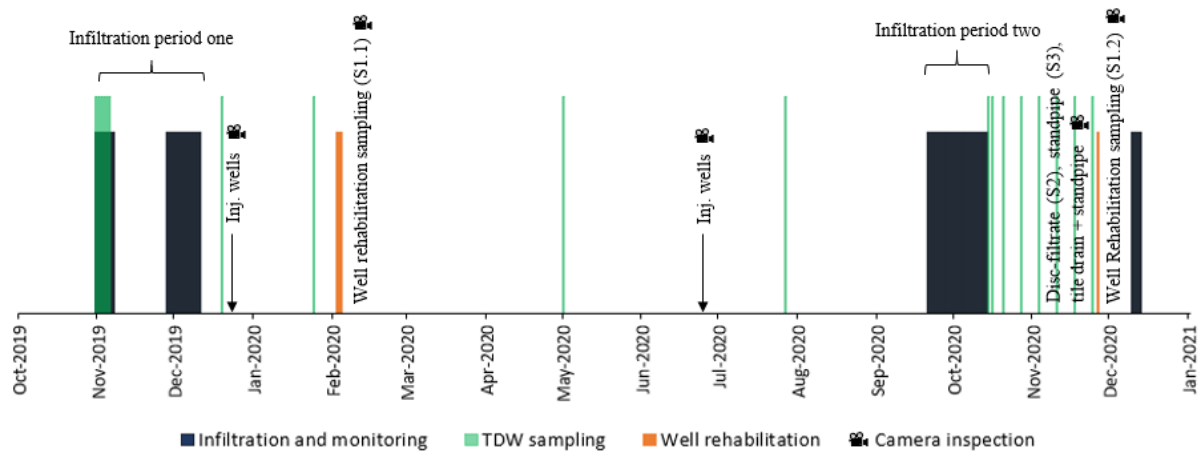


Figure 2.4: Timeline of the study indicating the two monitored infiltration periods, well rehabilitation, and corresponding sampling information as summarized in Table 2.1.

Table 2.1: Summary of the performed analyses related to annotated monitoring and sampling points in Figure 2.4.

Monitoring/sampling	Analysis	Additional Information
<i>Standpipe</i>	Turbidity, DO, camera inspection	Sensors in standpipe
<i>Injection and monitoring well</i>	Temperature, water level	Dataloggers in gravelpack piezometer
<i>TDW</i>	pH, EC, DOC, ICP-MS, IC, Alkalinity	Sampled during discharge event from the drain reservoir (n = 19)
<i>Stagnant water in ASTR piping</i>	Turbidity, smell	24 th January 2020, faucet under disc-filters
<i>S1.1</i>	Fluid: pH, EC, temperature, turbidity, DOC, ICP-MS, IC Solid: C/N, 69% HNO ₃ digestion and ICP-MS, mineral identification & quantification, XRD, particle size analysis, digital microscope	Well rehabilitation sampling (n = 17) 2 nd to 4 th February 2020. Camera inspection before and after regeneration procedures
<i>S2</i>	Digital microscope	Disc-filtrate sampling (n = 5) 25 th November 2020
<i>S3</i>	Digital microscope	Material in standpipe sampling (n = 2) November 25 th , 2020
<i>Main tile outlet</i>	Camera inspection	3-minute discharge event
<i>S1.2</i>	Digital microscope	Well rehabilitation sampling (n = 3) 26 th November 2020

3. Results and Discussion

This section discusses the results obtained from events and procedures indicated by the study timeline (Fig. 2.4). The first subsection presents the extent of the clogging problem from the two monitored ASTR injection periods. The physicochemical properties and characteristics of tile drainage water are subsequently discussed in the next subsection. The viability of the 40 μm spin Klin-disc filters is evaluated in relation to the clogging mitigation guidelines to assess the pre-treatment suitability. The following subsection presents the (hydro)geochemical and microscopic results on backflushed suspended material obtained during the well rehabilitation (S1.1 and S1.2). The clogging material and mechanisms are concluded by the contributed suspended solids during injection and the hydrochemical environment in the well. The well rehabilitation is subsequently discussed, evaluating the regeneration methods applied and proposing alternative rehabilitation methods to recover well performance. Finally, clogging mitigation strategies and recommendations on alternative pre-treatment are discussed to decrease the clogging potential.

3.1. Extent of the Clogging Problem

3.1.1. Infiltration Period One (October 31st to December 11th, 2019)

Figure 3.2 presents the injectivity index of infiltration runs supplied by field drainage events (Fig. 3.1). Generally, the injectivity decreased from approximately 6 m³/h/bar to approximately 2 m³/h/bar after infiltrating 1370 m³ per well over 20 days. This was caused by a decrease in recharge flow from 12 m³/h to approximately 4 m³/h because of an increase in head due to clogging.

At the beginning of the period, between October 31st to November 6th, both wells performed similar and showed a consecutive decrease in injectivity (head increase) with infiltration runs. As shown in Figure 3.3a and 3.3b, the conditions in the standpipe at the start of the ASTR operation measured relatively turbid conditions during the first few days. After a dry period between November 7th and November 28th, rainfall events supplied recharge water for a large infiltration run (approximately 20 h) on November 29th. Subsequent days until December 6th showed numerous short runs (1 h) and seemed too short to reach maximum head rise during infiltration. The runs, however, attained consecutive decreases in injectivity. Concurrently, the monitored standpipe turbidity showed a linear increase from approximately 3 NTU to approximately 8 NTU from November 29th to December 6th (Fig. 3.3a).

From December 6th to December 10th, precipitation events provided a continuous infiltration run lasting four days (Fig. 3.1 and 3.2). Initially, a higher injectivity was realized by reaching hydraulic equilibrium (>3 h infiltration), although, showing a rapid decrease until both wells reached a clogged state of 4 m³/h injection on December 10th. Well one for that matter, showed clogging occurred to a larger degree compared to well two as indicated by the slightly higher injectivity for well two. The sharp injectivity decrease showed clogging developed rapidly within both injection wells. Across the four-day infiltration duration, the turbidity within the standpipe generally did not exceed 12 NTU (Fig. 3.3a). Remarkably, however, two days prior to the large infiltration event, significant turbidity readings were noticed in the standpipe between December 4th and 6th. These turbidity peaks showed consecutive readings of 110, 10, 900, 70 and 30 NTU at standstill between short infiltration runs (Fig. 3.3c). The trends in turbidity indicated the standpipe was subjected to a substantial amount of turbidity causing material, that slowly settled within the standpipe during standstill. No significant precipitation events coincide with these turbidity readings (Fig. 3.1), as shown by the short peaks in injectivity until December 6th.

Regardless of reaching hydraulic equilibrium by a longer infiltration run (>3 h), all infiltration runs for injection well one show head increased within the gravelpack while head decreased at the distant monitoring well. Because clogging did not occur at the distant monitoring well, it was assumed a reduction in head at distance indicates a reduction in recharge flow due to clogging at the injection well. This shows that regardless of infiltration duration, clogging of the injection well occurred at every infiltration run as shown by the general decreasing injectivity with time in period one (Fig. 3.2).

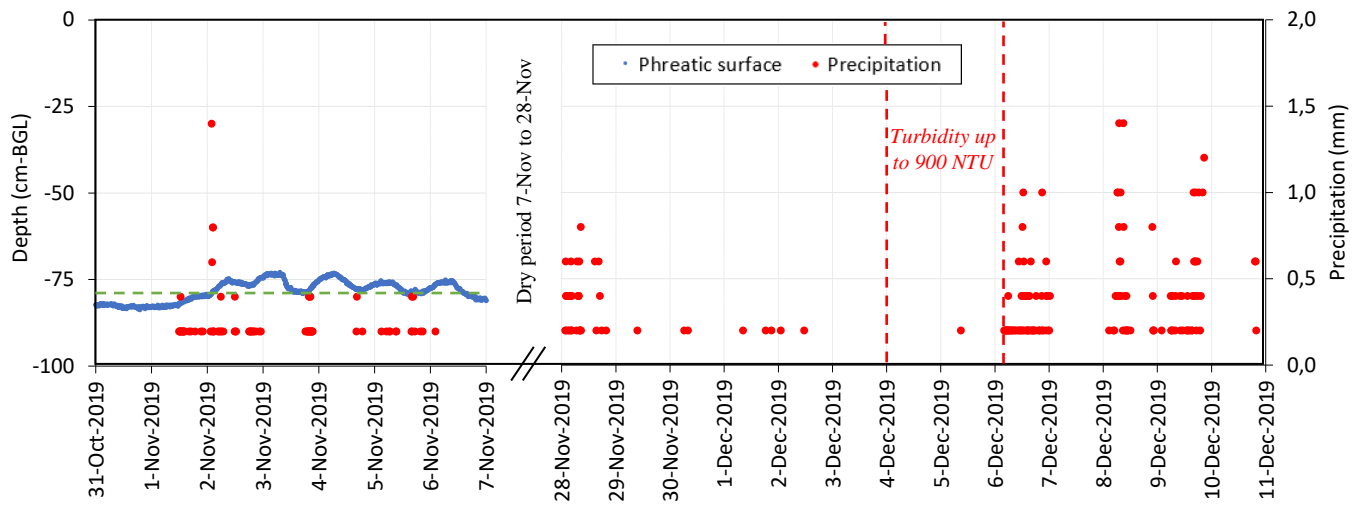


Figure 3.1: Precipitation (mm) and phreatic water level (cm-BGL) during infiltration period one. The green horizontal dashed line indicates the main tile depth at 80cm BGL. Phreatic water level data between 28-Nov-2019 to 11-Dec-2019 not available.

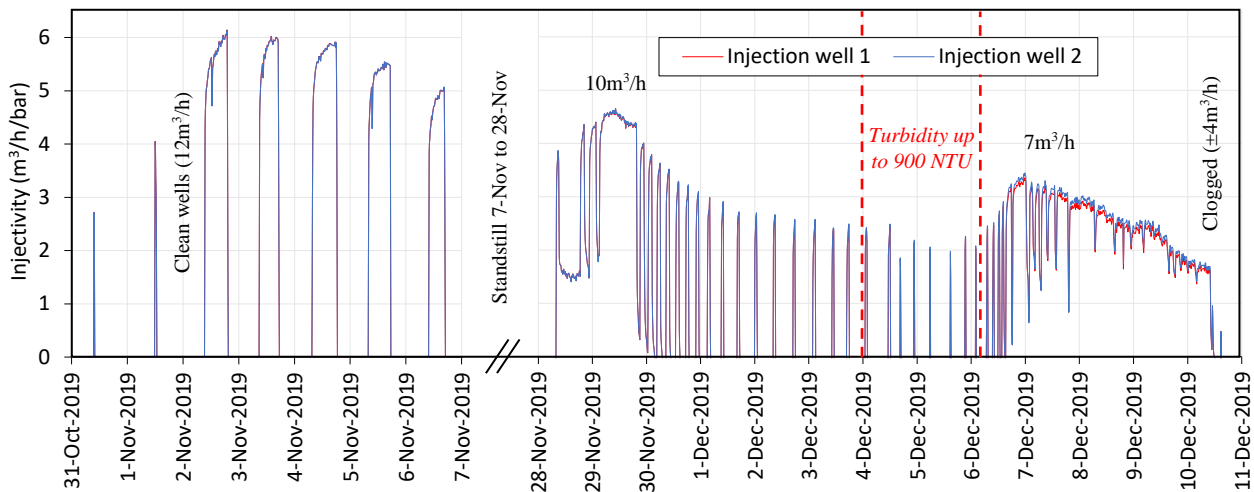


Figure 3.2: The decline in injectivity ($\text{m}^3/\text{h}/\text{bar}$) with time for injection well one and two during infiltration period one. Annotations provide information on operational conditions in black and implicating events in red.

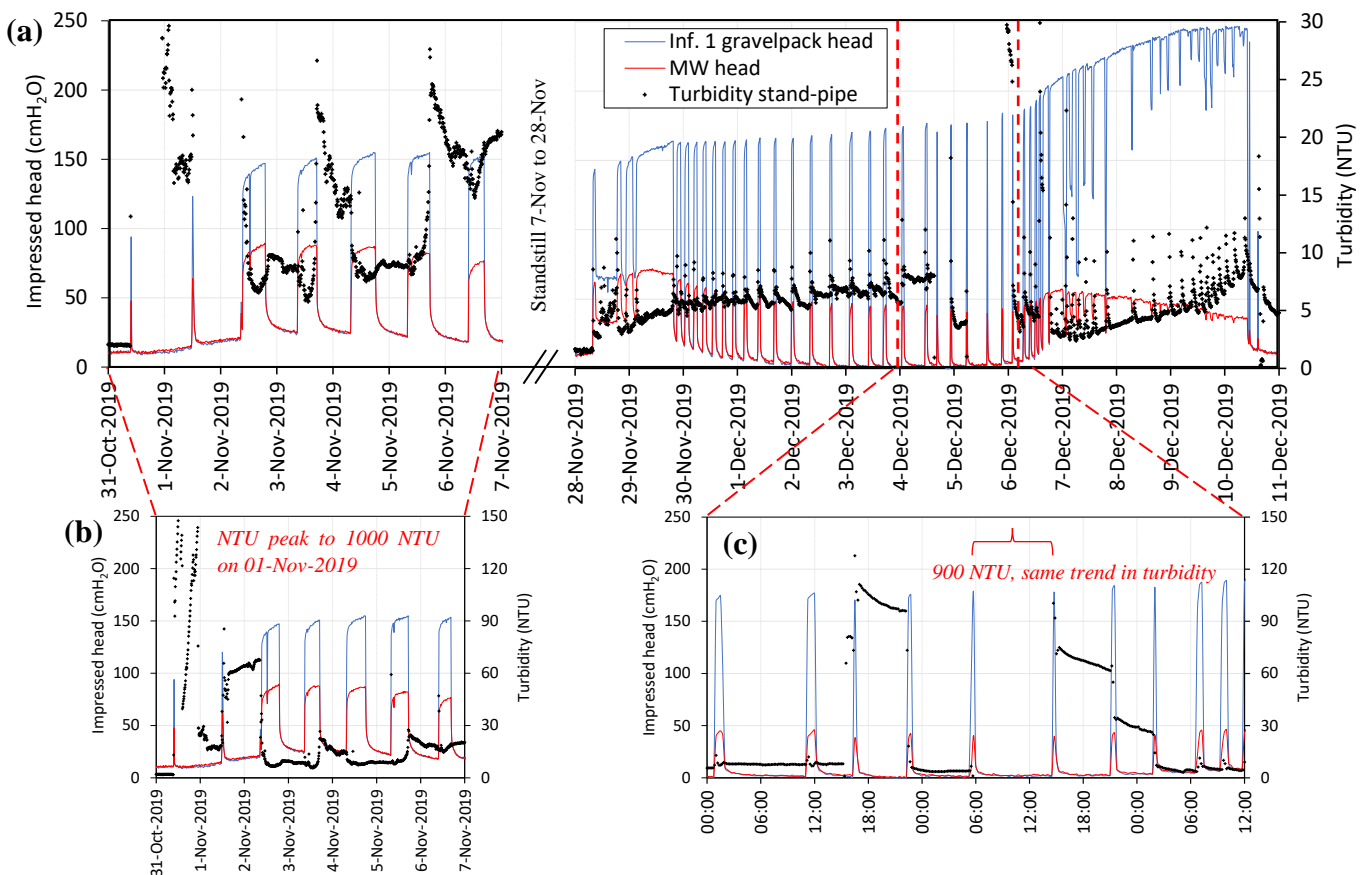


Figure 3.3: Plot 3.3a (top) shows the impressed head ($\text{cm H}_2\text{O}$) in the gravelpack piezometer of injection well one and the monitoring well at distance (7m), namely the abstraction well one gravelpack piezometer, in infiltration period one. The turbidity (NTU) in the standpipe is shown on the secondary y-axis. Plot 3.3b (bottom left) shows turbid events at the start of operation (31-Oct to 7-Nov-2019) See Fig. 2.3a in the supplementary data (SD) for turbidity peak to 1000 NTU. Plot 3.3c (bottom right) shows the extreme turbid events between 4-Dec to 6-Dec-2019. The turbidity event at 900NTU can be seen in SD. Fig. 2.3b.

Start of ASTR Operation (October 31st, 2019)

Remarkably high turbidity (up to 1000 NTU) in the standpipe was measured on the first two days of ASTR operation (Fig. 3.3b). The installed turbidity sensor within the drain reservoir at the main tile outlet allowed simultaneous turbidity monitoring in the drain reservoir and in the standpipe (Fig. 2.2). At the instance the ASTR system was turned on (December 10th, 2020), after a 56-day standstill, turbidity levels measured in the drain reservoir showed values around 5 NTU, while at the same instance, turbidity in the standpipe peaked at 600 NTU (SD. Fig. 3.4). On January 24th, 2020, after the system stood still for 60 days, stagnant water evacuated from the ASTR piping using the faucet showed water attained significantly turbid conditions. During the evacuation, an anoxic smell was additionally noticed, suggesting the stagnant water contained biological material. Turbidity levels at ASTR start-up on October 31st, 2019 showed these similar peaks in turbidity (Fig. 3.3b), with turbidity at 150 NTU.

Turbid Event December 4th to December 6th, 2019

Figure 3.3a shows the trend in turbidity before and after the extreme turbid event between December 4th and December 6th. In parallel, a zoomed in graph shows the remarkably turbid occurrence within the standpipe (Fig. 3.3c). It is unlikely the turbidity is primarily caused by loosened material within the ASTR piping because the system was already operating for several days. The turbid material, therefore, likely originated from the drain network in the field. Due to the fact no precipitation events occurred; the turbid event could be caused by maintenance practices on the tile drains. A discussion with a drain tile maintenance worker on site stated the heavy loads induced by tractors during land preparation can cause deformations in shallow subsurface tile drains. Slumps within in the tile drains consequentially provide locations for material to deposit and accumulate in the network. To counter these depositions, farmers perform a periodic drain flush intended to mitigate local drain clogging in the network and maintain proper functionality. Because no significant precipitation events occurred during the turbidity events, it is plausible the network was subjected to a suchlike flush during the two days event. Instead of discharging the turbid wastewater to the surrounding canal, it was discharged to the ASTR system and infiltrated.

3.1.2. Infiltration Period Two (September 20th to October 14th in 2020)

During the second infiltration period, both wells experienced an injectivity decrease from 5- to 1.5 m³/h/bar after infiltrating 1430 m³ per well over 20 days (Fig. 3.5). The well rehabilitation in February 2020 recovered the injectivity at the start of the infiltration period to 5m³/h/bar as shown on September 27th. From October 6th, an extreme rainfall event (80 mm/d) caused high water levels within the drain reservoir resulting in simultaneous infiltration and discharge to the surrounding canal. This is seen by the irregular injectivity patterns during the large infiltrated volume (approximately 700 m³ per well) between October 6th and October 11th (Fig. 3.5). Injection well two showed a larger rise in head rise within the gravelpack compared to well one. Indicating, on the contrary to infiltration period one, well two experienced more clogging in this period. This is also seen by the slightly higher injectivity for well one in the index. From late October 6th to October 11th, the turbidity in the standpipe consistently rose from 5 NTU to 160 NTU (Fig. 3.6) and seemed to cause two instantaneous reductions in injectivity (Fig. 3.5). First on October 8th followed by another event on October 11th. The recharge flow and impressed head decreased instantaneous during both events.

It was noticed the disc-filters experienced reduced functionality suggesting implications occurred within the pre-treatment system. The sudden reductions of injectivity was most likely caused by the reduced functionality of the disc-filters. Approximately 45 days after the system was shut down, camera inspections in the injection wells on November 25th indicated a large degree of filter slots were filled with material. Therefore, aside issues with the pre-treatment system, the observations implied the ASTR system also suffered from injection well clogging.

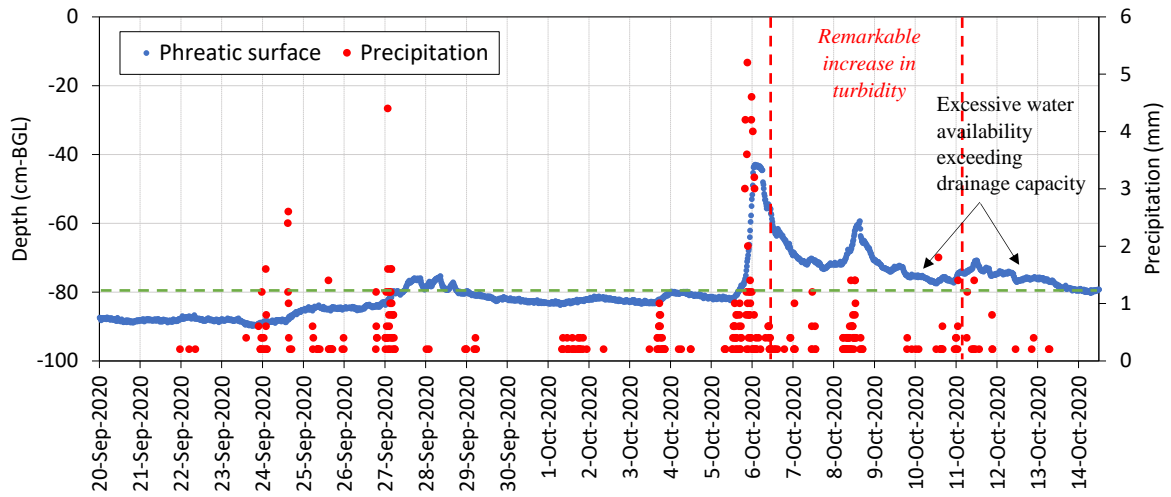


Figure 3.4: Precipitation (mm) and phreatic water level (cm-BGL) during infiltration period two. The green horizontal dashed line indicates the main tile depth at 80 cm BGL.

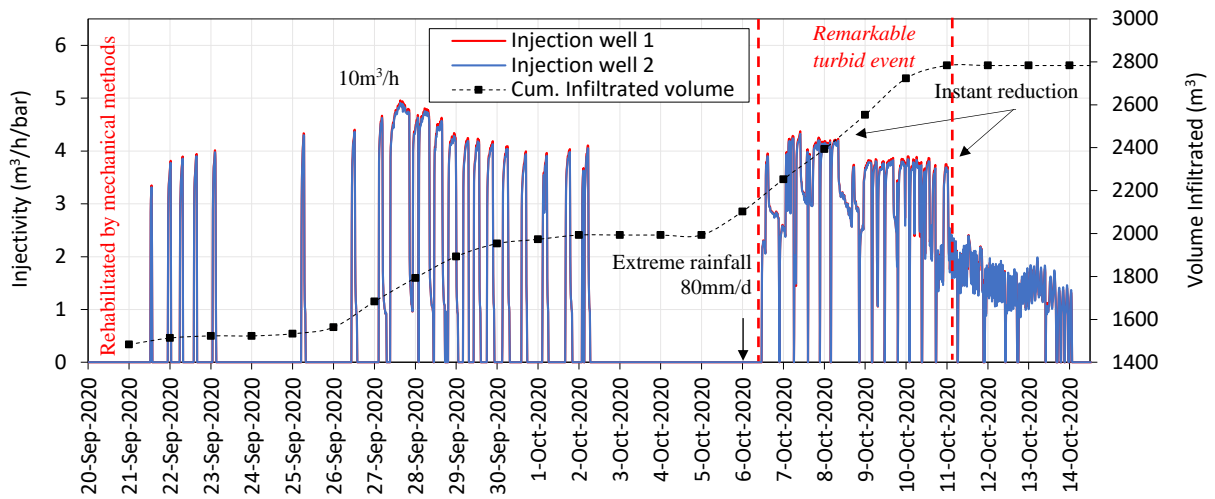


Figure 3.5: The injectivity index ($\text{m}^3/\text{h}/\text{bar}$) and accumulated volume infiltrated (m^3) per well with time for injection well one and two during infiltration period two. Annotations provide information on operational conditions in black and implicating events in red.

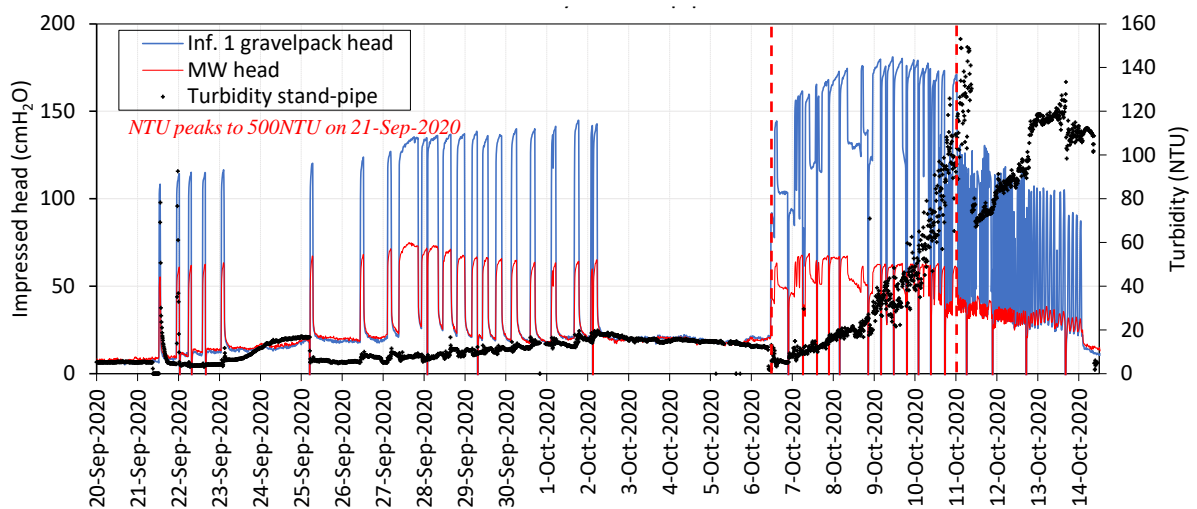


Figure 3.6: The impressed head ($\text{cm H}_2\text{O}$) in the gravelpack piezometer for injection well one and the monitoring well at distance (7 m), namely the abstraction well one gravelpack piezometer, for infiltration period two. The turbidity (NTU) in the standpipe is plotted on the secondary axis.

Start of ASTR Operation and Turbid Event Between October 6th and October 11th, 2020

Figure 3.6 shows the turbidity events in infiltration period two. At operational start-up on September 21st, 2020 peaks in turbidity were noticed up to 500 NTU. From October 6th, the large discharge event likely resuspended significant amounts of turbid material from the drain network. Over time, the material gradually flushed from the network and collected in the drain reservoir, subsequently discharged to the ASTR system.

3.1.3. Similarities and Differences between Infiltration Periods and Events

At the beginning of both infiltration periods at system start-up, remarkable peak values in turbidity were noticed within the standpipe. It is important to consider the possibility of introduced air bubbles at the instance the standpipe is filled at system start-up potentially causing these peaks ranging between 500 and 1000 NTU. Peaks in turbidity due to air bubbles are assumed to reach rather high NTU values and would be expected regularly by the frequent on/off operation. Figure 3.7a and 3.7b respectively show a typical turbidity and dissolved oxygen trend in the standpipe after the first few days of system start-up. Relatively small turbidity peaks (up to 10 NTU) are discerned at the instance an infiltration run starts, while dissolved oxygen decreases during standstill (~6 h). The decrease in dissolved oxygen indicates microbial (metabolic) processes occur within the ASTR system, since this reduction takes place regardless to introduced atmospheric oxygen within the stagnant standpipe water by diffusion. It is assumed the small peaks in turbidity seen in Figure 3.7a correspond to a flush of microbial particles, because similar observations were made of scoured suspended material in film footage within the tile drainage network when discharging from rest.

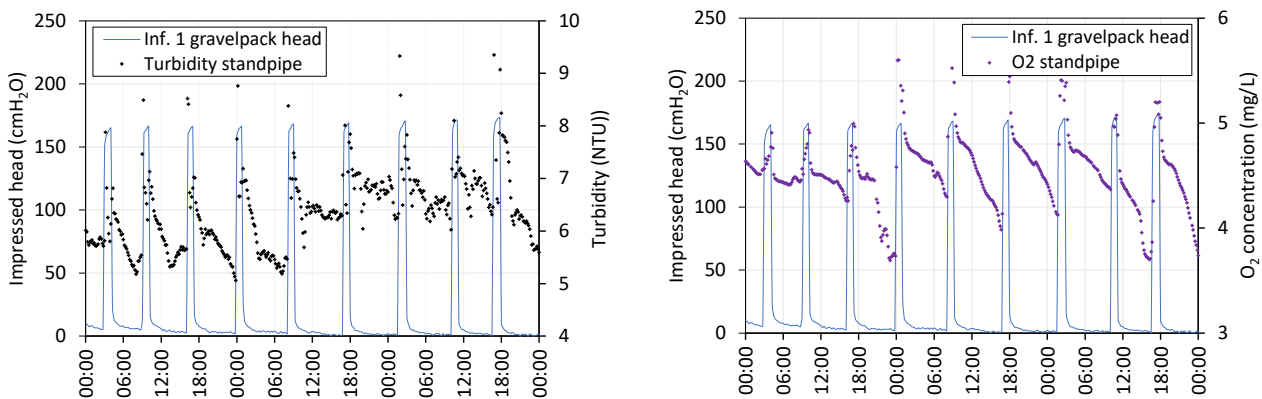


Figure 3.7: Plot 3.7a (left) and plot 3.7b (right) respectively show a typical pattern of turbidity (NTU) and dissolved oxygen (mgL^{-1}) during infiltration and standstill in the standpipe (1-Dec to 3-Dec 2019). A peak is noticed at the start of infiltration runs, while material settles in the standpipe during periodic standstill. During standstill, oxygen rapidly decreases regardless of introduced atmospheric oxygen in the standpipe.

Generally, the turbidity of recharge water increased over the duration of infiltration periods, as seen between November 28th to December 4th, 2019 (Fig. 3.3) and September 25th to October 2nd, 2020 (Fig. 3.6). As a result, the injection wells experience a reduction in injectivity (Fig. 3.2 and Fig. 3.5, respectively). When precipitation events caused large drain discharge events between December 6th to December 10th, 2019 (Fig. 3.1) and October 6th to October 11th, 2020 (Fig. 3.4) an increase in turbidity was again noticed, while an extensive turbidity increase (up to 160 NTU) occurred during the latter when rainfall events were extreme (80 mm/day). This formed a major difference between the two infiltration periods. The injectivity trend indicated a rapid yet linear decrease during the four-day infiltration event in infiltration period one (Fig. 3.2), while instantaneous reductions occurred during the five-day infiltration event in period two (Fig. 3.5). Because of the prolonged and excessive discharge amount, the instant injectivity reductions most likely related to reduced functionality of the disc-filters

by clogging when subjected to high turbid loads. Another difference relates to the new automated backflush system in period two providing periodic backflush events. As shown in Figure 3.8, the automated backflush events resulted in maintaining the injectivity with increasing turbidity load (blue) compared to period one (red). No automated backflush system in period one resulted in a rather rapid deterioration of the injectivity. The continued injectivity loss in period two from 2- to 1 m³/h/bar while undergoing the (intensified) automated backflush regime (backflush after infiltrating a volume of 50m³ per well), shows not all clogging material could be removed and material resided in the well.

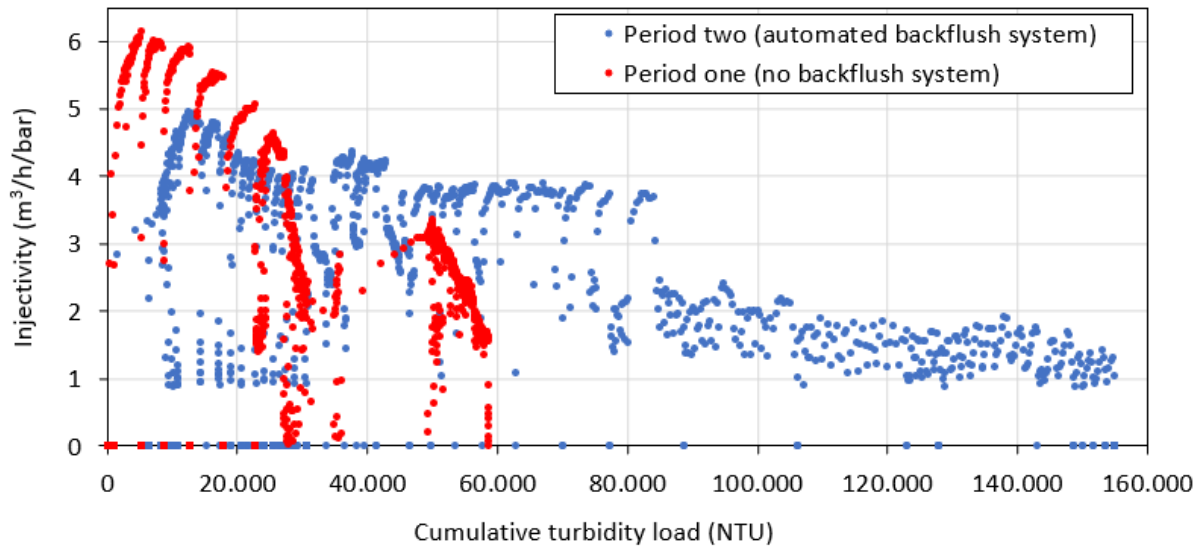


Figure 3.8: The injectivity versus the cumulative turbidity load for period two (blue) with the installed automated backflush system providing backflush, and period one (red) with no automated backflush system.

3.2. Results on the Injectant Water Quality and Suspended Material (Well Input)

This subsection first presents the hydrochemical properties of recharge water using saturation states to discuss the potential mineral precipitants. Subsequently, the physical and biological characteristics are discussed from microscopic result on samples. The retained material removed from the disc-filters and material removed from the interior of the standpipe provide information on the composition of suspended material in the injectant.

3.2.1. Hydrochemical Properties of Recharge Water

Hydrochemical properties show a nutrient-rich composition at circumneutral pH, with high concentrations of PO₄³⁻ (2-18 mgL⁻¹), SO₄²⁻ (117-350 mgL⁻¹), NO₃⁻ (6-50 mgL⁻¹), dissolved oxygen (2-6 mgL⁻¹), DOC (24.5-32.3 mgL⁻¹), NH₄⁺ (0.1-0.55 mgL⁻¹), Ca²⁺ (151-244 mgL⁻¹), K⁺ (50-74 mgL⁻¹), Mg²⁺ (25-40 mgL⁻¹), and Mn²⁺ (0.3-0.7 mgL⁻¹). A sample taken in duplicate in May 2020 evidenced the presence of particulate iron Fe³⁺ by analysing a filtered and unfiltered sample. The filtered sample measured 0.17 mgL⁻¹ Fe²⁺ while the unfiltered sample indicated total iron of 0.43 mgL⁻¹. The other 18 samples showed Fe²⁺ concentrations between 0.07 and 1.56 mgL⁻¹. The alkalinity (as HCO₃⁻) of recharge water is between 418 and 441 mgL⁻¹. The recharge water classifies as fresh with chloride concentrations between 105 and 122 mgL⁻¹ and EC between 0.9 and 1.0 mS/cm. The temperature of infiltration water is averaged at 12 °C, with approximately 14.5 °C in September to 9 °C in December. The SAR of injectant water is approximately 1.40. Considering the clogging mitigation guidelines, the infiltration water quality parameters regarding DOC, total iron, and nutrient like phosphate and ammonium, all exceed the guidelines and likely promote (bio)chemical clogging processes. Moreover, the presence of particulate iron likely contributes to physical clogging processes.

Saturation Indices and Potential Mineral Species

The saturation indices were calculated using PHREEQC assuming a temperature of 8°C and DO of 5 mgL⁻¹. The saturation state of hydroxyapatite (SI 6.7-8.5), ferrihydrite (SI 2.6-3), rhodochrosite (SI 0.3-0.8) and calcite (0.8-1.2) show the potential for precipitation of these minerals. It is important to note, however, the mineral equilibria and supersaturation should be interpreted with care. The presence of organic acids in groundwater are not incorporated and potentially impede the crystallization of these minerals. For example, fulvic and humic compounds may complex calcium, iron, phosphate, and magnesium and inhibit precipitation while modelling indicates clear supersaturation (Inskeep and Silvertooth, 1988; Stuyfzand, 2012). Moreover, most groundwater is close to equilibrium with calcite due to the presence of calcitic and aragonitic shell fragments in most marine formations (Stuyfzand and Raat, 2010). The shallow subsurface in Breezand, in that respect, contains a shell bed around the drain network, possibly influencing the saturation state for calcite. Organic acids and phosphates, on the other hand, may then again inhibit or cause sluggish calcite precipitation (Giannimaras and Koutsoukos, 1987; Apello and Postma, 2005). Lastly, kinetic hindrances play a significant role in, for example, rhodochrosite. The unaccounted complexation of Mn²⁺ by fulvic acids may be slow so that equilibrium is not attained (Jensen et al, 2002). Modelling does not regard the kinetics meaning interpretation of precipitants needs to be handled with utmost care.

Nevertheless, the well-known fast oxidation kinetics of Fe²⁺ (within hours at near-neutral pH when oxygen is not limiting) (Stumm and Morgan, 1996) and the presence of sampled particulate iron in recharge water indicate the precipitation of iron-oxide is occurring. The extensive studies conducted by works of van der Grift (2016) on, among other catchments; tube drain discharge with shallow groundwater tables in agriculture-dominated lowland catchments in the Netherlands, show particulate bound Fe-phosphate and Ca-phosphate (hydroxyapatite) formation is feasible. Similar observations are also made by works of Griffioen et al. (2006). Using methods of hydrogeochemical modelling and lab experiments on the aeration of nutrient-rich, anoxic groundwater near neutral pH, it was observed significant quantities of PO₄ immobilized in timeframes less than one day. The study also detected the immobilization could not solely be attributed to binding to iron-oxide types and concluded an association with calcium. The recent studies by Senn et al. (2015) rationalized the findings of Griffioen et al. (2006), showing the interdependent effects of phosphate, silica and calcium on the structure and composition of iron precipitates in near-neutral pH, bicarbonate-buffered aqueous solutions relevant for natural water resources. These extensive studies suggest sorptive and co-precipitation mechanisms most likely occur within the nutrient-rich recharge water along its flow path in Breezand.

The high affinity of phosphate with Fe(III) results in the predominant precipitation of Fe(III)-phosphate. Moreover, the presence of calcium likely associated with Fe(III)-phosphate to form Fe(III)-Ca-phosphate (Fe-hydroxyapatite) (Voegelin et al., 2010). Nevertheless, considering the saturation state of recharge water, the uptake of calcium to Fe(III)-phosphate could be inhibited by high concentration of DOC and the potential precipitation of calcite. Calcite, on the other hand, could precipitate sluggishly due to the high phosphate concentration. Finally, manganese-oxide precipitants in recharge water are feasible. Microbiology infers a strong interrelation on the chemical reactivity and precipitants in recharge water, specifically of iron and manganese in oxic groundwater (Tuhela et al., 1997).

3.2.2. Biological and Physical Characteristics of Recharge Water

The filamentous structures depicted in micrographs of sampled material retained on the disc-filters (Figure 3.9a and 3.9b) and material removed from the interior of the standpipe (Figure 3.10a and 3.10b) suggest the contribution of injecting biophysical material. The camera inspection within the standpipe after a 41-day standstill on November 25th, 2020 first showed a metallic sheen on the stagnant water surface before submerging the camera (SD. Fig. 5.1 and 5.2). Once submerged, an adhered mat covering the well interior was evident and revealed a thick structure of microbial deposits (SD. Fig. 5.3). The metallic sheen on the water surface is used as an indicator of iron-oxidizing bacterium present in nature (Emerson and de Vet, 2015). While the distinct morphology of filamentous structures associated with cells and the extensive formation of iron-flocs suggests the biochemical material consists of iron-oxidizing bacteria (FeOB) (Krempski et al., 2012; Emerson and de Vet, 2015). The conditions in the main tile outlet interior showed similar microbial structures as in the standpipe (SD. Fig. 5.5). This suggests the tile drainage system also contributes biochemical material to the recharge water, as sampled on the disc-filters. The significant biochemical material depicted support the rapid oxygen decrease in the standpipe in Section 3.1.3. When the ASTR system is stood still, the frequent on/off operation resuspends decayed or released material from within the drain network and ASTR piping, periodically increases turbidity.

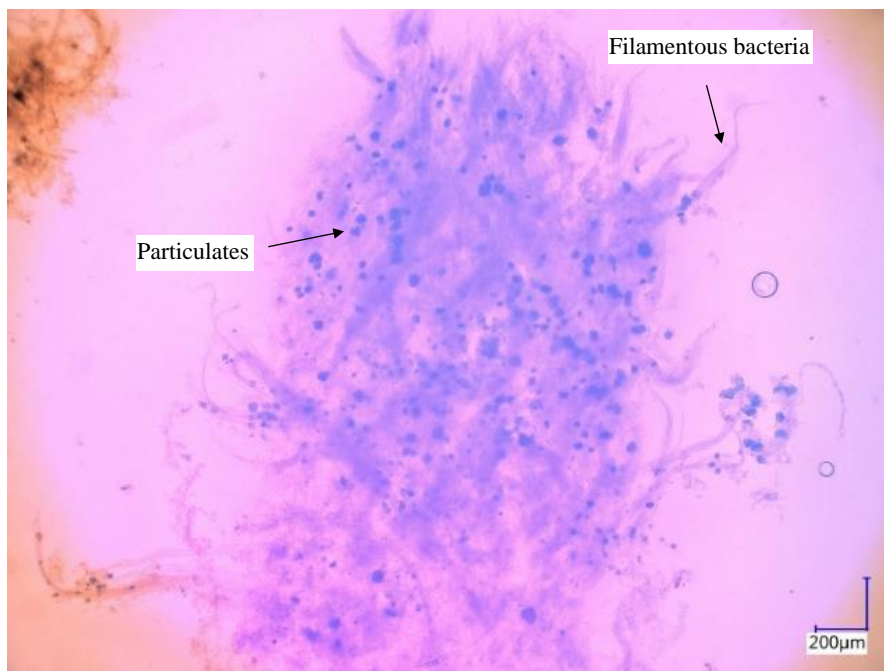


Figure 3.9a: Micrograph (x100 magnification – polarized) of material on disc-filters. Large (>1 mm) agglomeration of filamentous bacteria and particles.

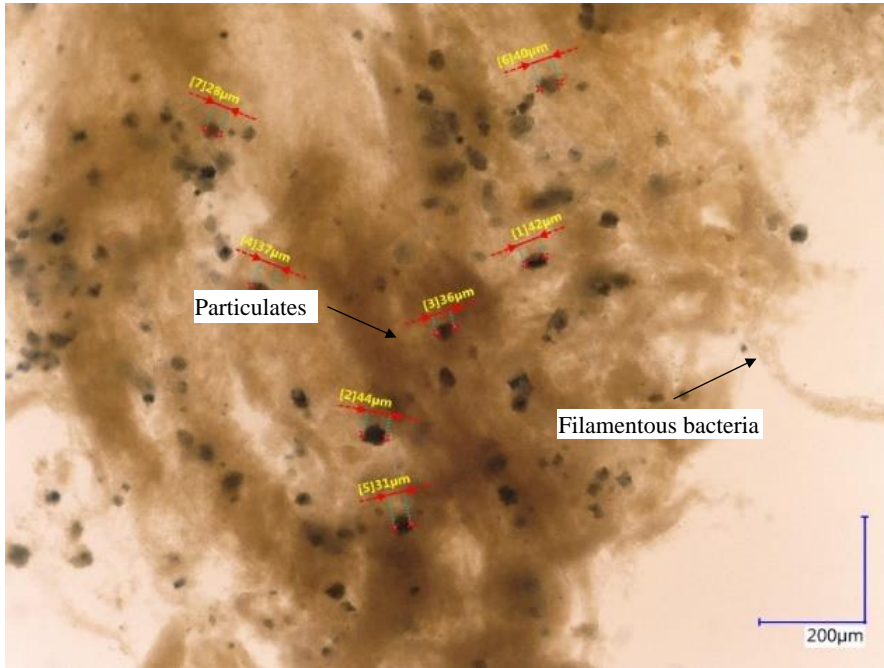


Figure 3.9b: Micrograph (x200 magnification) of material on disc-filters. Particles smaller and exceeding 40µm are depicted.

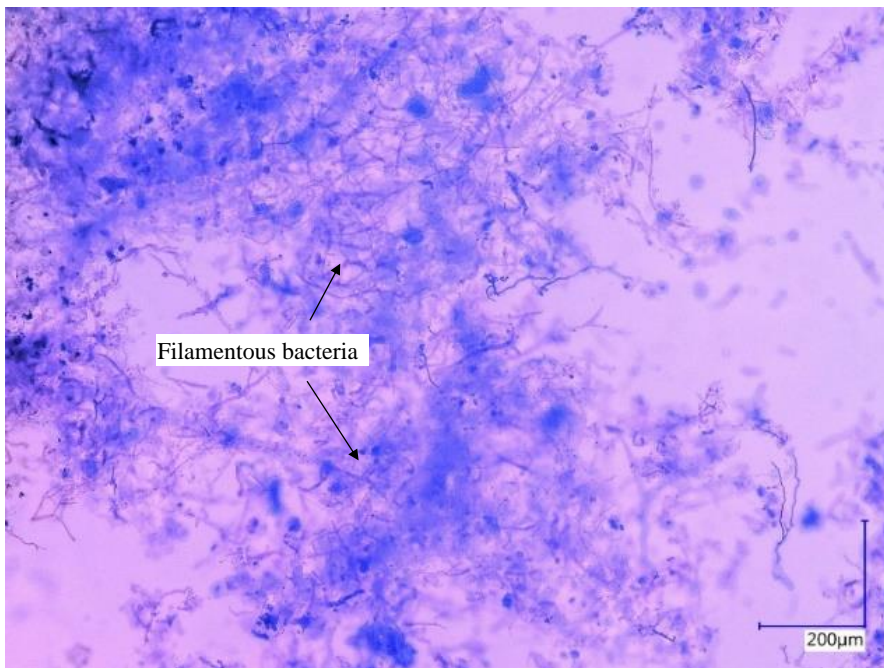


Figure 3.10a: Micrograph (x200 magnification – polarized) of material removed from the interior of the standpipe. An abundance of filamentous structures is depicted.

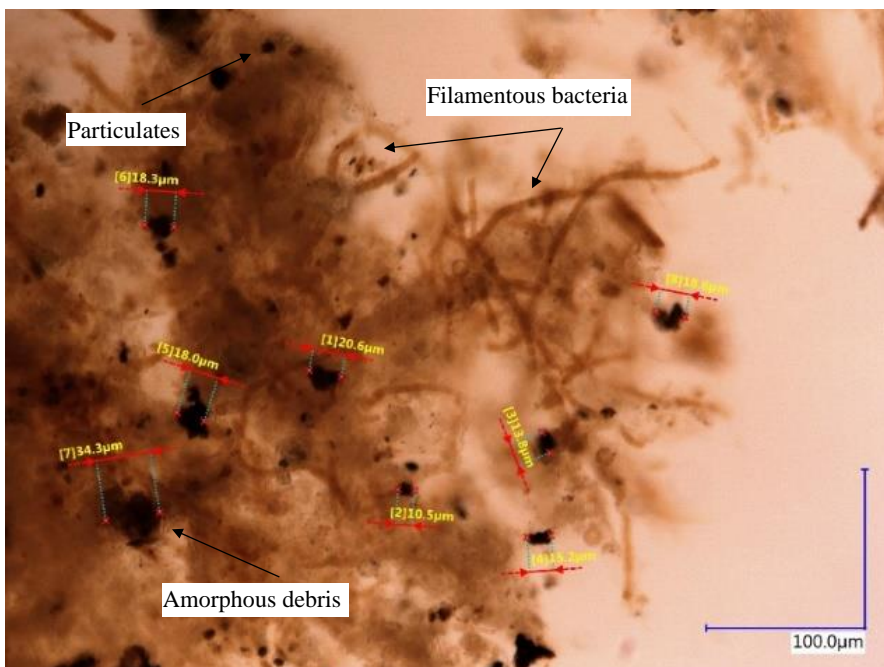


Figure 3.10b: Micrograph (x600 magnification) indicating particulates <40 µm incorporated by biochemical material (filamentous structures).

The micrographs show the bulk material contained filamentous structures and biofilm, incorporating amorphous flocs and particulates smaller and in exceedance of 40 μm in disc-filtrate and below 40 μm in standpipe material. The discrete particles are assumed to comprise of inorganic material like clay and silt incorporated in inorganic flocs. A simple acidification test ($\text{pH} < 3$) with 1% HNO_3 showed a significant reduction in bulk material, indicating a large portion of the bulk consists of metal-oxide flocs (SD. Fig. 7.6).

In conclusion, the nutrient-rich recharge water and organic carbon content promotes microbial growth within the ASTR system. It is assumed the suspended solids during infiltration comprise of organic ferric oxide structures complexed with phosphorus and calcium. Inorganic silicious particles such as clay and silts below 40 μm likely combine with labile organic material in the bulk material. The current 40 μm disc-filters allow flocs (between 15- and 40 μm) to pass, along with microorganisms and silicious particles below 40 μm . The turbidity and thus suspended solids can fluctuate considerably in the recharge water and increases over time during large drainage events. Biochemical floc formations (>40 μm) in the drain network are filtered out by the disc-filters and cause rapid clogging when subjected to large turbid loads. The high porosity and large specific area properties of iron oxides and hydroxide microstructures (Emerson and de Vet, 2015) passing the disc-filters enhance sorptive processes in the standpipe creating larger flocs as seen in Figure 3.9b. Similar turbidity causing processes occur within the tile drainage network by sorptive mechanisms between solutes that form flocs. During large precipitation events the biochemical material within the drain network is resuspended and flushed to the drain reservoir.

The susceptibility of biochemical processes in the ASTR piping system and drain network suggest similar microbial processes occur within the injection wells when infiltrating nutrient-rich oxic water. The biological processes within the injection wells result from introducing foreign microorganisms or stimulating the growth of indigenous organisms that accumulate cell biomass and secrete extracellular polymers (Maliva, 2020). Consequentially, siliceous particles, flocs and other microorganisms are captured by the biomass growth near filters slots and gravelpack, contributing to the clogging development.

3.3. Injection Well Clogging

The rising head with consecutive injection runs in infiltration period one (Figure 3.3) and period two (Figure 3.6) show the wells succumbed to severe clogging in a rather short time frame (20 d). The onset of clogging occurred at the instance operation started as seen by the direct successive head increase in the first few days of infiltration. The automated backflush events in period two successfully removed clogging material as seen by the relatively maintained injectivity (Fig. 3.8), but showed residual clogging remained evidenced by the slight decrease in injectivity and continued rise in head over time (Fig. 3.6). The trend in head rise in period one and two is linear for respectively the first 15 and 11 days, typical for physical clogging by infiltrating suspended solids (physical clogging). This is supported by the persisting head rise in the gravelpack and decreasing recharge flow indicative of clogging occurring at the borehole wall. This forms the primary location to filter injected particles by the fine-grained to medium-coarse aquifer interface (Olsthoorn, 1982). The impressed head rise during the relatively long infiltration periods of five days at the end of both periods showed the clogging rate increased significantly. The process continued to attain a linear process suggesting a significant contribution of suspended material (turbid load) during large recharge volumes.

Aside clogging at the borehole wall, significant clogging of filter slots occurred as seen by the camera inspection along the well screen after clogging event one. It is assumed biomass accumulation and microbial growth at the filter slots and gravelpack was promoted during short cycles of infiltration and standstill, possibly scouring biophysical material in the well by the frequent on/off operation filtered out at the borehole wall. This release of dead bacteria particles is similar to the processes observed

within the ASTR standpipe. Longer infiltration runs supplied an abundance of nutrients in the well, likely promoting additional biological growth. Clogging by physical processes, however, seemed dominant. This is supported by the lack of resistance decrease after the 21-day standstill in period one (no automated backflush system). An ASR system in Spangen, Rotterdam, concluded clogging of the injection well occurred predominantly due to biological instead of physical mechanisms (Zuurbiër and van Dooren, 2019). The resistance decrease after three to 30 days of standstill periods most likely resulted in the die-off of microbes, naturally rehabilitating the well performance once infiltration commenced (automated backflush after injecting 20 m³ at 30 m³/h for 5 minutes). In Breezand, the microbial decay during the 21-day standstill in period one showed no improvement in operation, suggesting physical clogging was dominant. Camera inspection in the injection wells since the well rehabilitation on June 19th, 2020, however, showed dark material filled the filter slots (SD. Fig. 8.4), predominantly in the upper well after a 140-day standstill. Hence, clogging by biological mechanisms attributes to the overall clogging development during longer standstill periods (>1 month). The residual clogging and localization of clogging after automated backflush events is discussed further in Section 3.4.3.

3.3.1. Results of Hydrogeochemical Analysis of Suspended Material (Well Output)

In Table 3.1, the main identified and quantified minerals (>1% d.w.) removed by the regeneration procedures are listed by applying equation (1) and converted to their oxide form. For the suspended material backflushed, the highest contents of main constituents follow, in decreasing order: Si (underestimated due to use of the oxidizing leach causing incomplete extraction), C_{org.}, Fe, P, S and Ca. Other constituents regarding Na, K, Mn, Mg, and Sr were <0.2% d.w and excluded.

The organic carbon bound sulphur and phosphorus was assigned with ratios of S:C = 0.018 (Stuyfzand and Osma, 2019) and P:C = 0.016 (Tipping et al., 2016), respectively. The rest of the organic carbon was assigned to soil organic matter (SOM) by a factor 2 (Prybil, 2010). The high sulphur content most likely indicates the presence of iron sulphide particles (pyrite) (Stuyfzand and Osma, 2019), originating from the target aquifer (Pers. Comm. Stuyfzand). Leaving the excess iron to be assigned to non-pyrite reactive minerals like iron-oxides, siderite, or vivianite (Griffioen et al., 2015). The remaining phosphorus, iron, and calcium content probably associate to form complex species. Hence, the minerals are categorized in Fe(OH)₃, CaCO₃, and PO₄ as main forms presenting an overestimation due to the complexation. Remaining % d.w. corresponds predominantly to SiO₂ and H₂O which is present in the crystal lattice of various minerals. An XRD analysis on a backflushed sample identified calcium carbonate with minor enrichment of magnesium (6.4%) (SD. Fig. 7.4). It is thus assumed a segment of the identified calcium can be assigned to a dominantly pure (93.6%) calcite composition likely originating from the target aquifer (Pers. Comm. Stuyfzand). Calcite could, however, also be contributed to the removed suspended material by infiltrating calcitic particulates present in drainage water or be a secondary precipitant during injection essentially coating aquifer fines considering the positive SI_{calcite} of the injectant.

No clear trends with depth could be deduced from the identified and quantified suspended material removed during the mechanical cleaning procedure. The data in Table 3.1 shows minerals removed predominantly consisted of SOM and pyrite. All horizons contained elevated contents of SOM and pyrite although the large amount of sediment removed hindered a relatively accurate identification of minerals. For most horizons, the sulphur exceeded the iron content, meaning no information on Fe(OH)₃ was obtained. After assigning sulphur to pyrite, the excess sulphur could only be related to sulphur-bearing particulates collected by corrosive properties of piping and machinery components used during the mechanical procedure (van Beek, 2010). Other minerals such as gypsum were neglected, as the hydrogeochemical conditions do not suffice this mineral formation.

Table 3.1: Analytical results on identified and quantified minerals of suspended material sampled during the well rehabilitation for injection well one and two. The first column summarises the regeneration phase and corresponding sample information.

Well Rehabilitation – Clogging Material								
Sample Information			Minerals					
Regeneration phase	Sample no.	Standing well = 270 L	SOM	Pyrite	Fe(OH)₃	CaCO₃	PO₄	Sum
		Approximate pumped volume/well screen sample location	%d.w.	%d.w.	%d.w.	%d.w.	%d.w.	%d.w.
Injection Well 1								
Initial backflush	1	90 L	33.4	7.8	13.0	11.1	21.0	86.4
	2	450 L	23.8	7.6	9.1	12.3	16.9	69.7
	3	720 L	22.6	7.6	22.7	11.1	30.0	91.0
	4	1440 L	22.1	8.0	39.6	9.4	40.8	120.0
Mechanical cleaning (jetting)	1	above filter	4.0	5.9	0.0	0.0	4.2	14.0
	2	top filter	4.5	5.4	0.0	0.8	4.2	15.0
	3	middle filter	2.3	0.7	0.0	2.5	0.5	6.1
	4	¾ filter	10.3	10.2	2.0	3.4	9.9	35.8
	5	bottom filter	3.4	4.2	0.0	8.8	1.8	18.2
Post backflush	1	300 L	8.8	5.3	1.3	8.7	8.2	32.3
	2	1260 L	0.0	0.0	0.0	0.0	0.0	0.0
Injection Well 2								
Initial backflush	1	90 L	38.6	22.0	6.1	9.2	28.8	104.8
	2	450 L	38.6	19.5	12.3	10.2	32.0	112.6
	3	1440 L	22.1	14.9	50.2	10.3	45.5	143.1
Mechanical cleaning	1	¼ filter	8.1	11.0	1.8	2.0	10.0	32.8
Post backflush	1	90 L	18.8	9.0	19.9	7.4	27.1	82.2

3.3.2. Hydrochemical Environment in the Well

A remarkable difference in hydrogeochemical properties were noticed in the analysis of successive backflush samples in time. After pumping approximately 700 L, a change in water quality indicated a distinction in water type, predominantly between water in the well and surrounding the well screen in the gravelpack as schematized in Figure 3.10. The water within the well prior to the backflush procedure was stagnant, considering the substantially clogged filter slots (95%) and the recharge rate of 4 m³/h at the end of infiltration period one. The conditions within the well since the shutdown (82-day standstill) became anoxic (reflected by the absence of O₂ and NO₃⁻ practically absent) with a sulphate reduced environment of approximately 20% compared to surrounding water. Upon removing the well heads, a foul H₂S gas was noticed. The environment attained significantly raised HCO₃, DOC, Mn²⁺, Fe²⁺, PO₄³⁻, Ca²⁺, Sr²⁺ and As³⁺ compared to surrounding water (respectively¹: HCO₃⁻: 640 vs. 450 mgL⁻¹, DOC: 48 vs. 25 mgL⁻¹, Mn²⁺: 580 vs. 420 µgL⁻¹, Fe²⁺: 3500 vs. 45 µgL⁻¹, PO₄³⁻: 37 vs. 12 mgL⁻¹, Ca²⁺: 220 vs. 175 mgL⁻¹, Sr²⁺: 1100 vs. 700 µgL⁻¹ and As³⁺: 40 vs. 16 µgL⁻¹). The suspended

material, on the other hand, showed an inverse trend to the fluid phase, showing lower particulate Fe^{3+} and P content in the well and higher content surrounding the well screen as listed in Table 3.1. The particulate calcium content, for that matter, remained relatively unchanged. The elevated HCO_3^- and DOC in the well coincided with elevated SOM content in suspended material removed from the well, compared to lower content surrounding the well screen. Various hydrochemical reactions in and proximally to the well occur during standstill. Reactions listed by Zuurbier et al. (2016) when injecting oxic injectant into the deeply anoxic aquifer are assumed relevant to processes occurring in the wells and target aquifer in Breezand.

Antoniou et al. (2012) found similar remarkable hydrogeochemical anomalies and processes when injecting oxic drinking water into a confined anoxic sandy aquifer in Herten, the Netherlands. The study concluded an anomalous increase of Fe^{2+} , Mn^{2+} and NH_4^+ in anoxic water measured within the gravelpack was caused by neo-formed organic material (microorganisms) after storage phases exceeded one month. Similar observations were made by Vanderzalm et al. (2006) on injecting oxic, nutrient-rich reclaimed water into a carbonate aquifer in Boliver, South Australia. It was concluded the Fe(hydr)oxides and Mn-oxides were used as an electron-acceptor for the mineralization of biomass around the ASR well. As the storage progressed, DOC, Fe^{2+} , Mn^{2+} , NH_4^+ and P concentrations increased in the well. This was presumed by the oxidation of immobile organic matter via de decay of biomass and any remaining particulate organic matter. Moreover, well rehabilitation studies reviewed by Gonzalez (2013) at three ASR system in the Netherlands injecting drinking water into a siliciclastic sand aquifer, identified elevated Fe^{2+} and Mn^{2+} concentrations in the well. It was concluded the mobilization occurred by reductive dissolution of iron and manganese hydroxides during shut-down periods.

During standstill, significant microbial activity catalyse hydrogeochemical processes in Breezand as seen by the elevated DOC, high SOM content in the well, and turbid standing well water conditions. The reduction of iron and manganese-oxides deposited in the well led to the mobilization of Fe^{2+} and Mn^{2+} . Concurrently, mobilization of P associated to iron-oxides can occur under reducing conditions (Mayer and Jarrel, 2000). The sulphate reduction by organic material (sulphate-reducing bacteria) is indicated by the H_2S gas release. The dissolution of calcite can also occur through bacterial mediation increasing calcium concentrations (Pfeiffer et al., 2000), likely by reduced primary carbonate precipitants proximally to the well or reduced Fe-hydroxyapatite contributed by the injectant.

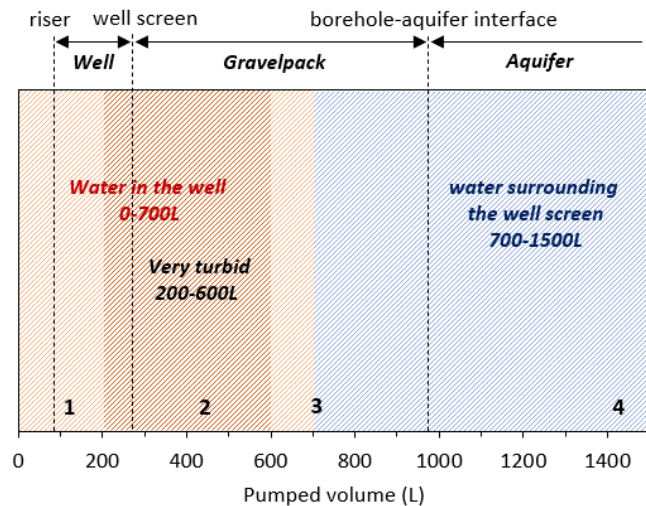


Figure 3.10: Schematic providing information on approximate backflush volumes and sampling points. Volume of riser, well screen, and well bore are respectively (accumulated): 90, 270, and 970 L. Sampling was done after pumping 90, 450, 720 and 1440 L, denoted by the numbering. Camera inspection during sampling showed a significant amount of suspended matter removed pumping 200-600 L. The material likely corresponded to removed material from the gravelpack and accumulated material at the bore bottom.

3.3.3. Results on Particle Size and Microscopic Analysis of Suspended Material

Figure 3.11a and 3.11b show a typical particle size analysis for the first backflush and mechanical cleaning procedure, respectively. Injected silicious clay and silt was removed in the first backflush samples together with flushed aquifer fines as shown by the peak at 10-20 μm and 200 μm , respectively. The peak at 250 μm for samples taken during the mechanical cleaning show predominantly aquifer fines were removed, supported by the poorly graded distribution.

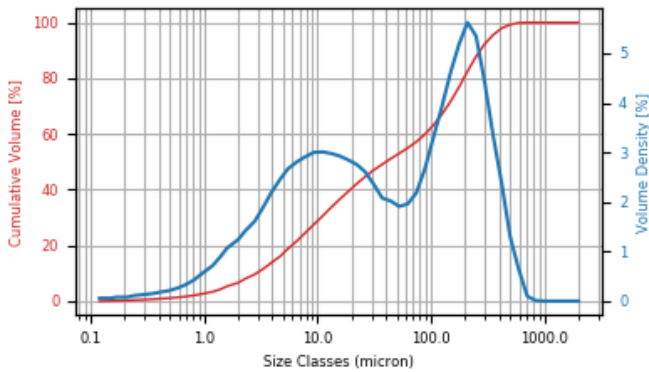


Figure 3.11a: Typical particle size analysis for the regeneration backflush sample in February 2020. The peak at 10-20 μm likely represents injected clay and silt while the peak at 200 μm corresponds to flushed aquifer fines.

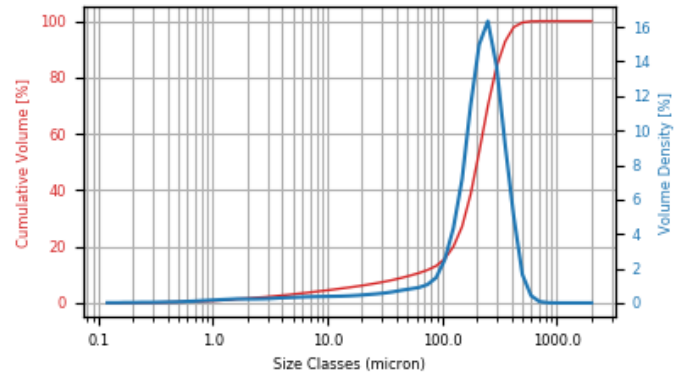


Figure 3.11b: Typical particle size analysis for the mechanical cleaning sample in February 2020. The peak at 250 μm and poor graded distribution suggest the predominant removal of aquifer fines.

Figure 3.12a and 3.12b show micrographs of suspended material removed during the mechanical cleaning procedure in February and November 2020, respectively. Brown/orange flocs incorporating particulates below 40 μm and microorganisms were depicted. Aside filamentous bacteria, disc-shaped bacteria of 50-60 μm size were seen (protozoa: soil testate amoebae (Foissner and Korganova, 1995)).

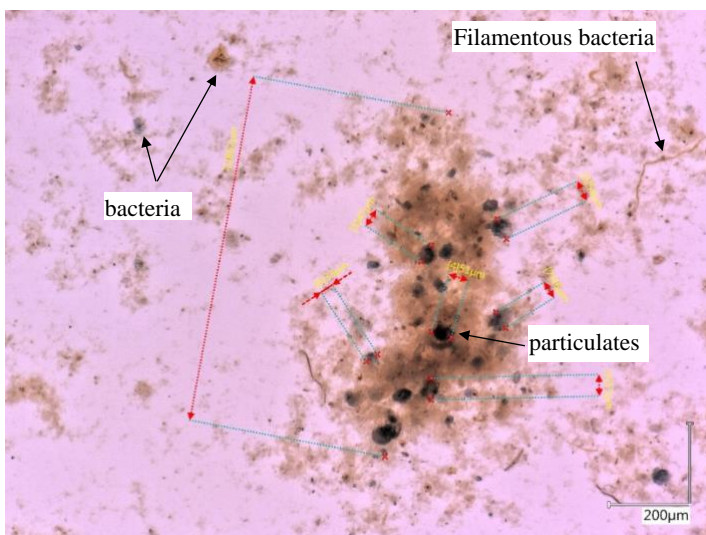


Figure 3.12a: Micrograph (x200 magnification) of suspended material removed during the mechanical cleaning on February 3rd, 2020. A large floc (~860 μm) incorporates particulates 30-50 μm . Bacteria are depicted.

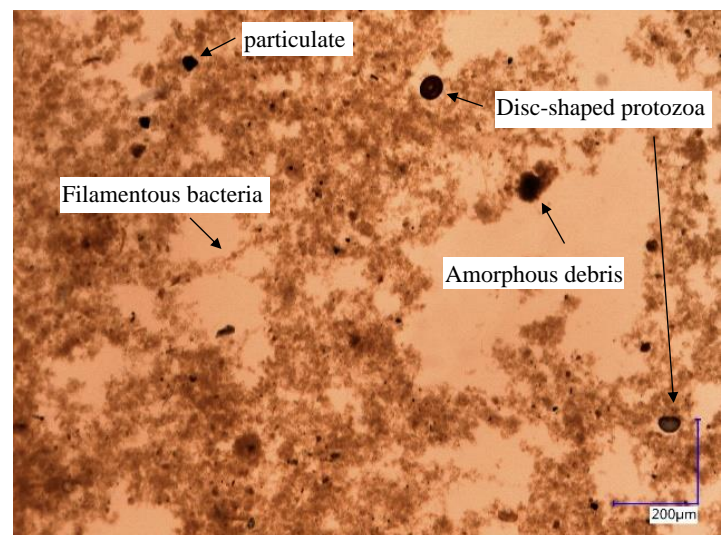


Figure 3.12b: Micrograph (x200 magnification) of suspended material removed during the mechanical cleaning on November 25th, 2020. Amorphous debris, filamentous bacteria, disc-shaped protozoa, and (few) particulates are depicted.

3.3.4. Clogging Material Composition

The clogging material is of young age, considering the 42-day infiltration period and 82-day stillstand. The hydrochemical analysis concludes numerous hydrogeochemical processes took place within the well, predominantly by microbial processes. Therefore, accurately predicting the clogging mineralogy in time is difficult, especially in the absence of hydrogeochemical modelling. Nevertheless, the bulk clogging material consists of soil organic matter such as microorganisms (biomass) agglomerated with the contribution of infiltrated silicious clay and silt debris, $\text{Fe}(\text{OH})_3$, Fe-hydroxyapatites, hydroxyapatite, and possibly calcite particulates.

3.4. Well Rehabilitation Evaluation

3.4.1. Camera Inspection

Figure 3.13 and 3.14 show the clogged and rehabilitated state of the injection wells by the regeneration methods applied. The long filter screen (21.5 m) showed internal well staining of predominantly ochreous (orange/brown) and dark (black/grey) material. Filter slots were filled 95% with both ochreous and dark material. As Olsthoorn (1982) states, regeneration with high-pressure jetting is suitable for removing material from filter slot, while proving less effective for removing clogging material at the borehole wall. The rehabilitation indeed showed near to complete recovery of filter slots, while at certain horizons internal well staining remained. Large sections of filter screen showed very clean conditions, effectively rehabilitated by the high-pressure jetting procedure.



Figure 3.13a: Clogged state after infiltration period one. Image is of the top filter case, taken on February 2nd, 2020.



Figure 3.13b: Clogged state of the lower filter case, taken February 2nd, 2020.

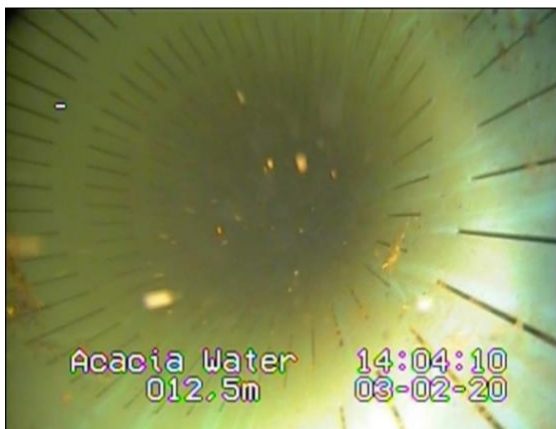


Figure 3.14a: In-well condition after the well rehabilitation. The horizon is the exact same as figure 3.13a, indicating 12.5m due to faulty camera calibration.



Figure 3.14b: In-well condition after the well rehabilitation. Horizon is the exact same as 3.13b.

3.4.2. *Operational Improvement and Considerations*

An assessment on filter slot resistance decrease was done by the service provider (Q-Flow International B.V.). A pumping test after the full rehabilitation showed a resistance decrease of approximately 90% for the filter slots (between the well and the gravelpack piezometer). The well performance recovery could only be assessed by the following infiltration period in September 2020. Considering both injection wells at the first infiltration period showed a head rise of 100 cm H₂O in the gravelpack piezometer with clean wells (October 31st, 2019, Fig. 3.3a), well one proved successfully rehabilitated by a substantial reduction in head in the gravelpack at the start of infiltration period two (from 250- to 110 cm H₂O, respectively (Fig. 3.3a and 3.6)). Moreover, the recharge flow showed a recovery from approximately 4 m³/h to approximately 10 m³/h per well. Well two for that matter, showed a less effective rehabilitation and operated with higher resistance (from 160- to 140 cm H₂O, respectively (SD Fig. 2.2 vs. 3.2)). Considering the filter slots were fully cleaned, it suggests the remaining resistance is probably caused by residual clogging within the gravelpack and borehole wall.

Automated backflush system

The automated backflush system maintained injectivity as shown in Section 3.1.3. A slight reduction in resistance (head in gravelpack piezometer) after backflush events indicated easily removed clogging material was effectively removed to some extent. Residual material did, however, remain as seen by a gradual resistance (pressure) increase with consecutive backflush events. The increasing drawdown with successive backflush events indicated clogging material was residing at the borehole-aquifer interface (SD. Fig. 3.1 and 3.2).

Flushing of aquifer fines

Section 3.3.3 shows aquifer fines (200-300 µm) are flushed through the relatively coarse gravelpack material (800-1200 µm) during a backflush event. This may prove beneficial in removing clogging material filtered out on the intersecting aquifer borehole wall during infiltration (Olsthoorn, 1982). However, removing aquifer fines in large quantities can cause disturbance to the surrounding aquifer matrix, which can result in compaction of the target aquifer leading to deteriorated hydraulic well performance over time.

3.4.3. *Residual Clogging Material*

Residual clogging probably consisted of trapped inorganic particles by the persistence of biological growth in the gravelpack and borehole wall. While chemical clogging by secondary calcite precipitants could contribute as discussed in Section 3.3.1.

3.4.4. *Alternative Regeneration Methods*

In time, a (major) rehabilitation is needed to remove the residual clogging and fully rehabilitate the well performance. Rehabilitating by methods of high-pressure jetting followed by compressed-air ‘jutteren’ can prove effective in removing material from the borehole wall, gravelpack, and filter slots (Olsthoorn, 1982). Juttering consists of creating a shockwave through a sudden pressure drop. This is performed by forcing the water level in the well downwards and opening a quick-acting valve on the closed well head with simultaneous air-lift pumping. A significant abstraction flow is realised loosening clogging material immediately. If mechanical regeneration methods are not effective in fully restoring well performance, chemical treatment should be applied. Clogging of the injection wells in Breezand due to injecting organic material (microorganisms) and inorganic material (iron and manganese flocs) and accumulating biomass by biological processes appoints acid treatment with an oxidizer and

subsequent redactor as suitable (Olsthoorn, 1982; Martin, 2013). Organic material like biological slimes usually encapsulate inorganic material, suggesting a strong oxidant (H₂O₂) and subsequent acid treatment (HCl) could be effective. A combined application of an acidic oxidant like HNO₃ could also provide viable results (Gonzalez, 2013). Rehabilitating both injection wells in Breezand merely with high-pressure jetting costs approximately €3,800. Applying compressed-air jutteren totals to €6,400 and applying chemical treatment during jutteren totals to €11,600.

A timeline to anticipate for a (major) rehabilitation could be implemented by following the generic model proposed by Dillon et al. (2016). A rehabilitation regime is constructed using operational variables linking the clogging rate (acute and residual), volumes infiltrated and backflush volumes. A (major) rehabilitation is required when the volume of water backflushed exceeds a determined factor times the volume of water injected in the previous cycle.

3.5. Clogging Mitigation Strategies for Breezand and Similar ASTR systems

Reducing or mitigating the susceptibility of injection well clogging when infiltrating to an anoxic sandy aquifer can be achieved by treating the recharge water to preventative guidelines values. Table 3.2 lists the considered parameters in this study showing turbidity, total iron, and DOC in TDW do not reach recommended values, as indicated by the exceedance factor. Reducing the injected suspended material (metal oxide flocs, organic particles such as microbes, and silicious clay and silt particles) is paramount to reduce the physical clogging potential. Reducing the dissolved oxygen content in recharge water may result in less extensive microbial metabolism causing biomass accumulation and the mediation of Fe and Mn oxidation. However, no recommended guideline values in literature are known for phosphate, nitrate, and dissolved oxygen to reduce biological clogging potential. In a geothermal system, a closed system prevents contact with oxygen otherwise resulting in excessive scaling and biological activity (Pers. Comm. Maren Brehme). For the ASTR application in Breezand, the original source of recharge water is rainwater with flow paths in natural open systems. As a result, the recharge water will likely maintain oxygenated conditions. It is recommended, however, to lower high concentrations of phosphate, nitrate, dissolved oxygen, and biodegradable organic material (like DOC) in MAR systems to reduce the biological clogging potential.

Table 3.2: A comparison of the recommended physicochemical clogging mitigation parameters to the TDW recharge water values investigated in this clogging study.

Clogging mitigation parameter (unit)	Recommended value	Breezand TDW value	N (samples)	Exceedance factor	Source
<i>Turbidity (NTU)</i>	< 5	5 – 160	Continuous	None to 32x	Martin (2013)
<i>Total iron (µg/L)</i>	< 10	430	1	43x	Zuurbier and van Dooren (2019)
<i>DOC (mg/L)</i>	< 2	24.5-32.3	17	12 to 16x	Zuurbier and van Dooren (2019)
<i>Ammonium (mg/L)</i>	< 0.5	0.1 – 0.55	17	No exceedance	Hubbs (2006)
<i>Phosphate (mg/L)</i>	Lower	2.0 – 18.3	19	-	Stuyfzand and Osma (2019)
<i>Nitrate (mg/L)</i>	Lower	6.1 – 50	19	-	Eom et al. (2020)
<i>Dissolved oxygen (mg/L)</i>	Lower	2 - 6	Continuous	-	Stuyfzand, Pers. Comm. (2021)
<i>Sodium Adsorption Ratio (-)</i>	< 6	1.40	4	No exceedance	Zuurbier and van Dooren (2019)

Two approaches are discussed to reduce physical and biological clogging potential for the Breezand ASTR system and similar future projects: (1) adjustments to the tile drainage network and ASTR system and (2), adjustments to the pre-treatment.

3.5.1. Tile Drainage Network

Steering infiltration on turbidity

It is apparent the source water supplied from the drain network can attain significantly turbid conditions (up to 160 NTU). Consequentially, implications at the disc-filters occur when the suspended material content becomes excessive. Therefore, steering discharge from the drain reservoir to the ASTR system on turbidity is a logical adoption strategy. Currently, the installed turbidity sensors (begin December 2020) has a threshold on 20 NTU. However, methods to reduce the turbid causing material within the tile drains need to be considered to ensure adequate recharge volumes can be utilized for injection instead of discharged to the surrounding surface water if turbidity constantly exceeds the threshold.

Reducing oxic conditions in the tile drainage network

In Breezand, atmospheric oxygen enters the tile drainage system at the main tile outlet in the drain reservoir (Fig. 2.2) maintaining oxic conditions in the tile drainage water. The main tile pipe is at a shallower elevation than the phreatic water level (Fig. 3.1 and 3.4) causing the full extent of the 400-m main tile pipe to be in direct contact with atmospheric oxygen. Mitigating contact with atmospheric oxygen may allow conditions within the network to reach anoxic conditions and reduce extensive biological oxidation and flocculation processes. As a result, less turbidity causing material may accumulate within the network when discharged to the ASTR system. Reducing the atmospheric oxygen in the drain network could be done by placing the tile drainage network at a deeper elevation in the topsoil. Considering the phreatic water level, placing the tile drainage network in the saturated zone together with a deeper drain reservoir allows the water level in the field to be regulated while submerging the main tile pipe. This should inhibit direct contact with atmospheric oxygen at the main tile outlet in the drain reservoir because the main tile pipe is fully submerged. The topsoil material, however, dependant on the cultivated crop, is of fine sand with relatively high hydraulic conductivity in Breezand, thus attaining low water retention. Opting such a design for future projects requires site-specific evaluation (topsoil: clay, peat, fine sand) on placing the tile drainage network deeper in the topsoil and retaining adequate water retention for crops. Moreover, when the ASTR system is not utilized, appropriate discharge regulation in the drain reservoir needs to be maintained to ensure field drainage remains effective. An advantage to a deeper tile drainage network in the topsoil also benefit any negative implications by field preparation practices. A deeper network is less susceptible to deformations or damage by heavy tractor loads. The viability of reaching an anoxic condition within the tile drainage network, however, is presumed low. Further investigation is warranted to evaluate results on achieving lower turbid loads during discharge.

3.5.2. Alternative Pre-treatment

An assessment on the turbidity reduction (%) by the current 40 µm Klin-disc filters in Breezand requires a calibration of the turbidity sensor in both the drain reservoir and standpipe (before and after the disc-filters). The turbidity sensors give sufficient information on turbidity trends over time, although the reading between the two turbidity sensors on March 18th, 2021 experienced a deviation of approximately +50% on a 25 NTU standard solution, and approximately +12% on a 100 NTU standard solution. This shows over time, the sensors experience a contaminating coating on the optical window implicating the accuracy of NTU readings to assess the disc-filters efficacy.

Nonetheless, the Klin-disc filters have proven to be unviable in reducing the physical clogging potential. A previous ASTR pilot (Acacia Spaarwater) injecting tile drainage water to the same aquifer utilized a pre-equalization tank (settling tank), followed by a slow sand filter. This led to an ASTR pilot experiencing a low physical clogging risk. Similarly, the pre-treatment scheme utilized by Zuurbier et

al. (2016) on injecting oxic rainwater run-off from greenhousing to an anoxic middle-coarse to very coarse sandy aquifer used a settling tank followed by rapid sand filtration and slow sand filtration. A constant specific infiltration capacity was maintained (no clogging) over the 20 months of operation. Therefore, adopting a settling tank followed by a rapid- and slow sand filter may prove feasible in reducing the physical and biological clogging potential in Breezand.

Treating recharge water with granular activated carbon is considered an effective method to reduce both physical and biological clogging by reducing turbidity and DOC (like AOC) in MAR applications (Page et al., 2011; Stuyfzand and Osmá, 2019). However, Bonte et al. (2009) related periodic standstill of ASR systems to an elevated AOC concentration released from the filters at operational startup. Considering the frequent on/off operation in an ASTR applications with tile drainage water, introducing additional AOC during injection should be prevented for biological clogging reasons. Moreover, the related costs to regenerating activated carbon are high, making the treatment option even less attractive. Applying a coagulant/flocculant like iron sulphate prior to sand filtration to reduce PO₄ in injectant is not recommended. Besides higher operational costs and maintenance of filters, the potential contribution of flocs into injection wells have been documented to enhance clogging development (Gonzalez, 2013).

4. Conclusion and Recommendations

The feasibility of the current ASTR pilot in Breezand injecting tile drainage water (TDW) in an anoxic brackish fine-grained to medium-coarse sandy aquifer is presumed low in regards to the risk of clogging. The TDW injectant attains a high clogging potential by physical mechanisms due to exceeding recommended clogging mitigation guidelines for suspended material (turbidity in recharge water usually between 5-20 NTU; up to 160 NTU. Mitigation guideline: 1-5 NTU). Moreover, the nutrient-rich water composition (PO₄: 2-18 mgL⁻¹, NO₃: 6-50 mgL⁻¹, NH₄: 0.1-0.55 mgL⁻¹, DOC: 24.5-32.3 mgL⁻¹) and dissolved oxygen content (2-6 mgL⁻¹) realise a high clogging potential by biological mechanisms. Due to the sorptive processes and co-precipitation between high concentrations of Fe, P, and Ca in TDW together with significant microbial processes in the tile drainage network, suspended material consists of organic Fe-hydroxyapatite flocs agglomerated with inorganic particles like siliceous clay and silt particles as seen in micrographs. The 40 µm Klin-spin disc filters allow biochemical material (15-40 µm) to pass. This results in the pre-treatment providing low impact to adequately reduce the high physical clogging potential as seen by the rapid clogging development (20 days) in both infiltration periods. During large precipitation events and prolonged drain discharge, the disc-filters are subjected to significant turbid loads by resuspended and scoured material from the tile drainage network. As a result, the operability of the disc-filters deteriorate due to clogging resulting in a lower injectivity for the ASTR system.

The ASTR pilot suffered predominantly from physical clogging mechanisms. This was concluded by the typical linear clogging process, the corresponding clogging location at the aquifer-borehole interface, the lack of resistance decrease after a standstill period (21 days), and the contribution of infiltrated particulates in removed suspended material (clogging material). The significant clogging of filter slots concluded by down-hole camera inspection, clogging in the gravelpack, deeply anoxic conditions in the well during standstill (> 1 month), and high SOM content in backflushed suspended material suggest clogging by biological mechanisms follow in dominance. Moreover, the microbial (metabolic) processes observed within the ASTR standpipe suggest similar conditions occurred within the well, further supporting the high potential for biological clogging. Distinguishing chemical clogging mechanisms from both physical and biological is difficult, although in-well flocculation forming iron and manganese oxides by the admixing of native groundwater is assumed less significant to the overall clogging contribution. The process likely occurs further away from the well at the mixing zone of oxic infiltrate and iron-rich native groundwater considering the relatively slow reaction kinetics. The

identified calcium carbonate in the clogging material likely resembles primary carbonate precipitants from the aquifer formation (likewise for identified pyrite). Calcium carbonate as a secondary precipitant is, however, feasible due to the positive SI_{calcite} of recharge water. Moreover, contribution of infiltrated calcitic particles in recharge water during infiltration is also a possibility. Mechanical clogging by entrained air is ruled out because the typical clogging process curve does not correspond. Clogging by clay swelling or mobilization cannot be ruled out but is assumed of low significance due to the practically absent clay content in the target aquifer and the small difference in SAR of injectant and native groundwater (1.4 to 0.8, respectively). A certain interdependency between physical and biological clogging in the well is feasible. The accumulation of $\text{Fe}(\text{OH})_3$ and MnO_2 in the well during injection may act as a food source for reducing bacteria during standstill, as seen by the significantly elevated Fe^{2+} and Mn^{2+} after standstill exceeded one month. It is thus assumed the order of clogging mechanisms in decreasing order follows: (1) physical, (2) biological, (3) chemical, and (4) mechanical.

The applied well rehabilitation method of mechanical cleaning (high-pressure jetting) proved effective in removing resistance over the filter screen slots. The injection well performance was, however, not fully recovered due to residual clogging on the borehole wall and gravelpack. It is advised to rehabilitate the wells with high-pressure jetting followed by compressed-air ‘jutteren’ to effectively remove clogging material from the filter slots, gravelpack, and borehole wall. The automated backflush system ensured the injectivity was adequately maintained in comparison to the first infiltration period without the automated backflush system.

To reduce the risk of clogging by physical and biological mechanisms in Breezand and similar future ASTR projects, it is advised to adopt a (closed) settling tank to collect and store discharged water from the irrigation field. As an alternative to the 40 μm Klin-disc filters, it is recommended to subsequently treat the TDW using a rapid- followed by a slow sand filter. This has proven to reduce the suspended material significantly and achieve recharge water of 1 NTU. Additionally, using the settling tank as pre-equalization tank allows the infiltration runs to be managed, controlled, and endure longer infiltration runs. This would reduce the frequency of on/off operation currently causing short infiltration runs that promote the flushing of dead microbe particles in the ASTR piping system (standpipe), essentially contributing to the injectant suspended solids. Moreover, it likely benefits the operability of the sand filters by avoiding anoxic zones in the filter bed during frequent standstill. This may otherwise result in the potential release of H_2S or NH_3 in the effluent contributing to the clogging development. Once the injectant suspended solid content attains a relatively constant concentration by adopting an effective pre-treatment, a representative MFI index can be determined. This allows optimized methods proposed by Stuyfzand and Osma (2019) to be applied to quantify physical injection well clogging. Achieving a better understanding of the microbial environment is done by DNA extraction on injectant suspended material and removed suspended material from the well. Regarding the accuracy of monitoring, periodic calibration of the NTU system sensors is advised to maintain accurate monitoring of the injectant properties. Lastly, attention for the governing laws regarding injectant water quality and environmental protection of groundwater bodies should be considered for the adoption of this water management technique. Norms set by ‘Kader Richtlijn Water’ (RIVM, 2006) concern the infiltration of $\text{NO}_3 < 50 \text{ mgL}^{-1}$ and total pesticides $< 0.5 \mu\text{gL}^{-1}$. While norms set by ‘Besluit Kwaliteitseisen en Monitoring Water’ (BKMW, 2009) limit TSS $< 0.5 \text{ mgL}^{-1}$, TP $< 0.4 \text{ mgL}^{-1}$, and $\text{SO}_4 < 150 \text{ mgL}^{-1}$ in preventing further contamination of groundwater bodies.

Cited References

- Antoniou, A., Breukelen, B.M., Stuyfzand, P.J., 2012. Hydrogeochemical patterns, processes and mass transfer during aquifer storage and Recovery (ASR) in an Anoxic Sandy Aquifer. *Applied Geochemistry* 27. 2435-2452.
- APHA (American Public Health Association), 2005. *Standard Methods for the Examination of Water and Wastewater*. 735 APHA-WEF-AWWA, Washington.
- Appelo, C.A.J., Postma, D., 2005. *Geochemistry, Groundwater and Pollution*, 2nd Edition. Amsterdam, the Netherlands
- Beek, C.G.E.M, 2010. Cause and Prevention of Clogging of Wells Abstracting Groundwater from Unconsolidated Aquifers. PhD dissertation, Vrije Universiteit van Amsterdam
- Bonte, M., Raat, K., Dammers, P., Stuyfzand, P.J., 2009. Verstopping en Regeneratie van Infiltratieputten bij Waalsdorp. H2O/7
- Bouwer, H. (2002) Artificial Recharge of Groundwater: Hydrogeology and Engineering. *Hydrogeology Journal* 10:121-142.
- Brehme, M., Regenspurg, S., Leary, P., Bulut, F., Milsch, H., Petrauskas, S., Valickas, R., Blocker, G., 2018. Injection-Triggered Occlusion of Flow Pathways in Geothermal Operations. *Geofluids Volume* 2018
- Camprovin, P., Hernandez, M., Fernandez, S., Martin-Alonso, J., Galofre, B., Mesa, J., 2017. Evaluation of Clogging during Sand-Filtered Surface Water Injection for Aquifer Storage and Recovery (ASR): Pilot Experiment in the Llobregat Delta (Barcelona, Spain). *Water* 2017, 9:263
- Dillon, P., 2005. Future Management of Aquifer Recharge. *IAH Commission on Management of Aquifer Recharge, Hydrogeol j* (2005) 13:3 13-316
- Dillon, P, Vanderzalm, J., Page, D., Barry, K., Gonzalez, D., Muthukaruppan, M., Hudson, M., 2016. Analysis of ASR Clogging Investigations at Three Australian ASR Sites in a Bayesian Context. *Water MDPI*
- Emerson, D., de Vet, W., 2015. The Role of FeOB in Engineering Water Ecosystems: A Review. *Journal AWWA* 107:1
- Eom, H., Flimban, S., Gurung, A., Suk, H., Kim, Y., Kim, Y.S., Jung, S.P., Oh, S. (2020). Impact of Carbon and Nitrogen on Bioclogging in a Sand Grain Managed Aquifer Recharge (MAR). *Environ. Eng. Res.* 25(6): 841-846.
- Foissner, W., Korganova, G.A., 1995. Prescription of Three Testate Amoebae (Protozoa, Rhizopoda) from a Caucasian Soil. *Arch Protistenkd.* 146: 13-28
- Farrell, C., Hassard, F., Jefferson, B., Leziart, T., Nocker, A., Jarvis, P., 2017. Turbidity Composition and the Relationship with Microbial Attachment and UV Inactivation Efficacy. *Science of the Total Environment*, 624L 638-647.
- Fuller C. C., Davis J. A. and Waychunas G. A., 1993. Surface chemistry of ferrihydrite: Part 2. Kinetics of arsenate adsorption and coprecipitation. *Geochim. Cosmochim. Acta* 57, 2271–2282.
- Giannimaras, E.K., Koutsoukos, P.G., 1987. The crystallization of calcite in the presence of orthophosphate. *J. Colloid. Interface Sci.* 116, 423-430
- Gonzalez, B., 2013. Clogging of Deep Well Infiltration Recharge Systems in the Netherlands. KWR Watercycle Research Institute, Nieuwegein, the Netherlands.
- Griffioen J., 2006. Extent of immobilisation of phosphate during aeration of nutrient-rich, anoxic groundwater. *J. Hydrol.* 320, 359–369.

- Grifioen, J., Klaver, G., Westerhoff, W.E., 2015. The Mineralogy of Suspended Matter, Fresh and Cenozoic Sediments in the Fluvio-Deltaic Rhine-Meuse-Scheldt-Ems Area, the Netherlands. An Overview and Review. *Netherlands Journal of Geosciences – Geologie en Mijnbouw* 95-1, 23-106.
- Grift, B., 2016. Geochemical and Hydrodynamic Phosphorus Retention Mechanisms in Lowland Catchments. PhD Dissertation, Universiteit Utrecht.
- Houben, G.J., 2002. Iron Oxide Incrustations in Wells. Part 1: Genesis, Mineralogy and Geochemistry. Federal Institute for Geosciences and Natural Resources (BGR) Stilleweg 2, D-30655 Hannover, Germany. *Applied Geochemistry* 18 (2003) 927-939
- Hubbs, S.A., 2016. Riverbank Filtration Hydrology: Impacts on System Capacity and Water Quality. In Proceedings of the NATO Advanced Research Workshop on Riverbank Filtration Hydrology, Bratislava, Slovakia, 7–10 September 2004; Springer: Bratislava, Slovakia, 2006.
- Inskip, W.P., Silvertooth, J.C., 1988. Inhibition of Hydroxyapatite precipitation in the presence of fulvic, humic and tannic acids. *Soil Sci. Soc. Am. J.*, 52, 941-946
- Jensen, D.L., Boddum, J. K., Tjell, J.C., Christensen, T.H., 2002. The solubility of rhodochrosite (MnCO₃) and siderite (FeCO₃) in anaerobic aquatic environments. *Appl Geochem* 17(4):503–511
- Jeong, H.Y., Jun, S.C., Cheon, J.Y., Park, M., 2018. A Review on Clogging Mechanisms and Management in Aquifer Storage and Recovery (ASR) Applications. *Geosciences Journal*, Vol. 22, No. 4, p. 667-679.
- Krempsi, S.T., Hanson, T.E., Chan, C.S., 2012. Isolation and Characterization of a Novel Biomineral Stalk-Forming Iron-Oxidizing Bacterium from a Circumneutral Groundwater Seep. *Environmental Microbiology* (2012) 14(7), 1671-1680.
- Maliva, R.G., 2020. Anthropogenic Aquifer Recharge. WSP Methods in Water Resources Evaluation Series No.5, Springer Hydrogeology.
- Martin, R., (ed.) 2013. Clogging Issues Associated with Managed Aquifer Recharge Methods. IAH Commission on Managing Aquifer Recharge, Australia.
- Mayer D. T. and Jarrell W. M., 2000. Phosphorus sorption during iron(II) oxidation in the presence of dissolved silica. *Water Res.* 34, 3949–3956.
- Mills, W.R., 2002. The quest for water through artificial recharge and wastewater recycling. Management of Aquifer recharge for Sustainability. In Proceedings of the 4th International Symposium on Artificial Recharge of Groundwater, Adelaide, Australia, 22–26 September 2002; Balkema Publishers: Adelaide, Australia, 2002.
- Olsthoorn, T.N., 1982. The clogging of recharge wells, main subject. KIWA Communications-71, The Netherlands Testing and Research Institute, Rijswijk, Netherlands
- Okubo, T., and Matsumoto, J., 1983. Biological clogging of sand and changes of organic constituents during artificial recharge. *Water Research* 17 (7), 813-812.
- Page, D., Miotlinski, K., Dillon, P., Taylor, R., Wakelin, S., Levett, K., 2011. Water Quality Requirements for Sustaining Aquifer Storage and Recovery Operation in a Low Permeability Fractured Rock Aquifer. *Journal of Environmental Management* 92 (2011) 2410-2418.
- Page, D., Bekele, E., Vanderzalm, J., Sidhu, J., 2018. Managed Aquifer Recharge (MAR) in Sustainable Urban Water Management. *Water MDPI*
- Parkhurst, D.L., Appelo, C.A.J., 1999. User's guide to PHREEQC (version 2): a computer program for speciation, batch-reaction, one-dimensional transport, and inverse geochemical calculations. Water-resources investigations report; 99-4259. U.S. Geological Survey: Earth Science Information Center, Open-File Reports Section [distributor], Denver, Colorado, USA.

Pavelic, P., Dillon, P. J., Barry, K. E., Herczeg, A.L., Rattray, K.J., Hekmeijer P., Gerges, N.Z., 1998. Well Clogging Effects Determined from Mass Balances and Hydraulic Response at a Stormwater ASR Site. In Third International Symposium on Artificial Recharge, Amsterdam, Holland, 21-25 September.

Pérez-Paricio, A., Carrera, J., & Von Christierson, B., 2001. Numerical modelling of clogging. In Artificial recharge of groundwater, European commission project ENV4-CT95-0071 Final Report (pp. 100-107). Luxembourg European Communities-European Commission Directorate-General for Research.

Pfeiffer, S.R., Ragusa, S., Sztajn bok, P., Vandeveld, T., 2000. Interrelationships Between Biological, Chemical, and Physical Processes as an Analog to Clogging in Aquifer Storage and Recovery (ASR) Wells. *Wat. Res.* Vol 34, No. 7 pp. 2110-2118.

Post, V. Personal Communication: Email contact (August 14, 2020)

Pribyl, D.W., 2010. A Critical Review of the Conventional SOC to SOM Conversion Factor. Department of Soil, Water, Climate, University of Minnesota, United States. *Geoderma* 156 (2010) 75-83.

Senn, A.C., Kaegi, R., Hug, S.J., Hering, J.G., Mangold, S., Voegelin, A., 2015. Composition and Structure of Fe(III)-precipitates formed by Fe(II) oxidation in water at near-neutral pH: Interdependent Effect of Phosphate, Silica and Ca. *Geochimica et Cosmochimica Acta* 162 (2015) 220-246.

Senn, A.C., Kaegi, R., Hug, S.J., Hering, J.G., Mangold, S., Voegelin, A., 2017. Effect of aging on the Structure and Phosphate Retention of Fe(III)-precipitates formed by Fe(II) Oxidation in Water. *Geochimica et Cosmochimica Acta* 202 (2017) 241-360.

Schipper, J.C., Verdouw, J., 1980. The Modified Fouling Index, a Method of Determining the Fouling Characteristics of Water. KIWA, Rijswijk, the Netherlands. *Desalination*, 32:137-148

Stikker, A., 1998. Water Today and Tomorrow, Prospects for Overcoming Scarcity. *Futures*, Vol. 30, No. 1, p.43-62

Stumm, W., Morgan, J.J., 1996. *Aquatic chemistry, Chemical Equilibria and Rates in Natural Waters*, third ed. Wiley, New York

Stuyfzand, P.J., 1993. *Hydrochemistry and Hydrology of the Coastal Dune Area of the Western Netherlands*. PhD dissertation Vrije Universiteit Amsterdam and KIWA afd. Onderzoek & Advies.

Stuyfzand, P.J., Wakker, J.C., Putters, B., 2005. *Water Quality Changes during Aquifer Storage and Recovery (ASR): Results from Pilot Herten (Netherlands), and their Implications for Modeling*. ISMAR 5, Berlin, Germany. United Nations Educational, Scientific and Cultural Organization, pp. 164–173.

Stuyfzand, P.J., Raat, K.J., 2010. Benefits and hurdles of using brackish groundwater as a drinking source in the Netherlands. KWR Watercycle Research Institute, Nieuwegein, the Netherlands. *Hydrogeology Journal* 18:117-130

Stuyfzand, P.J., 2012. *Hydrogeochemical, for storage, management, control, correction and interpretation of water quality data in Excel spread sheet*, KWR, VU University of Amsterdam

Stuyfzand, P.J., Osmar, J., 2019. *Clogging Issues with Aquifer Storage and Recovery of Reclaimed Water in the Brackish Werribee Aquifer, Melbourne, Australia*. Water MDPI.

Susser, P., Schwertmann, U., 1983. Iron oxide mineralogy of ochreous deposits in drainpipes and ditches. *Z. Kulturtechnik Flurbereinigung* 24, 386–395.

Tipping, E., Somerville C.J., Luster, J., 2015. The C:N:P:S Stoichiometry of Soil Organic Matter. *Biogeochemistry* (2016) 130: 117-131.

Torkzaban, S., Vanderzalm, J., Treumann, S., Amirianshoja, T., 2015. *Understanding and Quantifying clogging and its management during injection of CSG water permeates, brines and blends*. Australia: CSIRO.

- Tuhela, L.; Carlson, L.; & Tuovinen, O.H., 1997. Biogeochemical Transformations of Fe and Mn in Oxic Groundwater and Well Water Environments. *Journal of Environmental Science and Health, Part A: Toxic/Hazardous Substances and Environmental Engineering*, 32:2:407.
- Vanderzalm, J.L., Le Gal La Salle, C., Hutson, J.L., Dillon, P.J., 2002. Water quality changes during aquifer storage and recovery at Bolivar, South Australia. In: *Management of Aquifer Recharge for Sustainability*, pp. 83–88.
- Voegelin A., Kaegi R., Frommer J., Vantelon D. and Hug S. J., 2010. Effect of phosphate, silicate, and Ca on Fe(III)-precipitates formed in aerated Fe(II)- and As(III)-containing water studied by X-ray absorption spectroscopy. *Geochim. Cosmochim. Acta* 74, 164–186.
- Walton, N.R.G., 1989. Electrical Conductivity and Total Dissolved Solids – What is Their Precise Relationship? *Desalination*, 72: 275-292.
- Wang, Z., Du, X., Yang, Y., and Ye, X., 2012, Surface clogging process modeling of suspended solids during urban stormwater aquifer recharge. *Journal of Environmental Sciences*, 24, 1418–1424.
- Zuurbier, K.G., Hartog, N., Stuyfzand, P.J., 2016. Reactive transport impact on recovered freshwater quality for a field MPPW-ASR system in a brackish and geochemically heterogeneous coast aquifer. *Applied Geochemistry* 71 (2016) 35-47.
- Zuurbier, K.G. and van Dooren, T.C.G.W., 2019. *Urban Waterbuffer Spangen*. KWR, Nieuwegein, the Netherlands.